A total of 128 decay curves were averaged, visualized, and saved by a digital oscilloscope (Hitachi Oscilloscope V-1065, 100 MHz; Hitachi Denshi, Ltd., Tokyo, Japan). Decay time constants were determined by computer-fitting the averaged decay curves to a single exponential,[26] using the Stern–Volmer equation and predetermined parameters of τ and kq corrected for the prevailing systemic blood pH and the temperature (29°C) in the window chamber. Since in anemia, pH may be lower than the systemic value, and considering that the quenching time constant increases by about 8% as pH varies from 7.2 to 6.2, interstitial Po_2 may be slightly overestimated.

Microcirculer Po_2 measurements were made 10 min after dye injection. The reflection coefficient for albumin in subcutaneous connective tissue is in a range of 0.8–0.9, causing a natural and continuous steady extravasation of albumin, which yields a measurable steady-state concentration of the albumin-bound porphyrin complex about 20–30 min after injection. The material appeared to be evenly distributed in the interstitium, since there was no evidence of significant variability in signal strength in the interstitium unrelated to the presence of underlying blood vessels after the initial equilibration of 20–30 min.

Data analysis

Data are expressed as the mean ± standard deviation (SD) for the indicated number of animals. Data were analyzed using analysis of variance (ANOVA) followed by Fisher's protected least significant difference (PLSD) test between the groups. Student t test was used for comparisons within each group. The level of confidence was placed at 95% for all experiments.

RESULTS

Rheological properties of PEG-HbV/HSA and HbV/HSA

When the unmodified HbV was dispersed in saline (Hb; 10 g/dL), the viscosity of the vesicular suspension became 2.6 cP at 358 s^{-1} (Fig. 2).[15] Dispersion in 5% albumin solution to adjust the colloidal osmotic pressure raised the 10 HbV/HSA viscosity to 8 cP at the same shear rate, which was higher than that of blood (3.7 cP at the same shear rate). All suspensions exhibited nonlinear behavior when tested *in vitro* as a function of shear rate, and these non-Newtonian characteristics were typical for particle suspensions. The 10 HbV/HSA had higher viscosity at lower shear rates owing to vesicular aggregation. The curve of 10 PEG-HbV/HSA was almost identical to that of human blood and had a viscosity of 3.5 cP.

Changes in systemic parameters during hemodilution

Hematocrit before the exchange was about 45% and was reduced to about 7% after exchange for all groups (Table II). There was no significant difference between the groups. The actual levels of blood exchange calculated from the hematocrit were about 29%, 62%, and 85%, for theoretical values of 30%, 60%, and 80%, respectively.

The HSA group started to show a significant decrease in MAP at 20% exchange (Fig. 3) and dropped to 38 ± 9 mm Hg (baseline 102 ± 6 mm Hg) for the last exchange. There was some MAP increase for the HbV/HSA and PEG-HbV/HSA groups at the first 10% or 20% exchange stages. The HbV/HSA groups showed transient abnormal high MAP (e.g., 140 mm Hg; data not shown), probably owing to high flow resistance caused by the high viscosity of HbV (8 cP). The 5 HbV/HSA and 5 PEG-HbV/HSA groups tended to decrease in MAP (e.g., 82 ± 11 and 84 ± 9 mm Hg, respectively, at 80% exchange) in comparison with the 10 PEG-HbV/HSA and 10 HbV/HSA groups. However, significantly ($p < 0.001$) higher MAP was observed for all the PEG-HbV and HbV groups compared to the HSA group, even after the completion of blood exchange.

The heart rate of the HSA group increased to a maximum 456 ± 32 beats/min at 50% exchange (baseline 405 ± 58 beats/min), probably owing to a cardiac output increase, and then decreased significantly to 306 ± 76 beats/min at 80% exchange owing to cardiovascular insufficiency consequent to anemia (Fig. 3). The 10 HbV/HSA and 10 PEG-HbV/HSA groups showed a transient significant decrease in heart rate at the first 10% exchange (Δ = −22 and −33 beats/min on average, respectively). However, they recovered at 20% or 30% exchange, and 10 HbV/HSA had the most

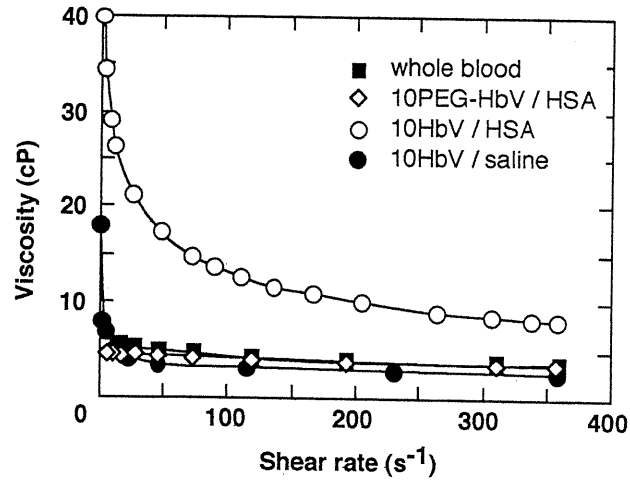

Figure 2. Shear rate dependence of the viscosity of 10 HbV-PEG/HSA, 10 HbV/HSA, 10 HbV/saline, and human blood measured with a capillary rheometer at 37°C. Unmodified HbV suspended in saline shows low viscosity. When it is suspended in HSA, the viscosity increases dramatically, especially at lower shear rates. On the contrary, PEG-modified HbV shows significantly reduced viscosity comparable with blood.

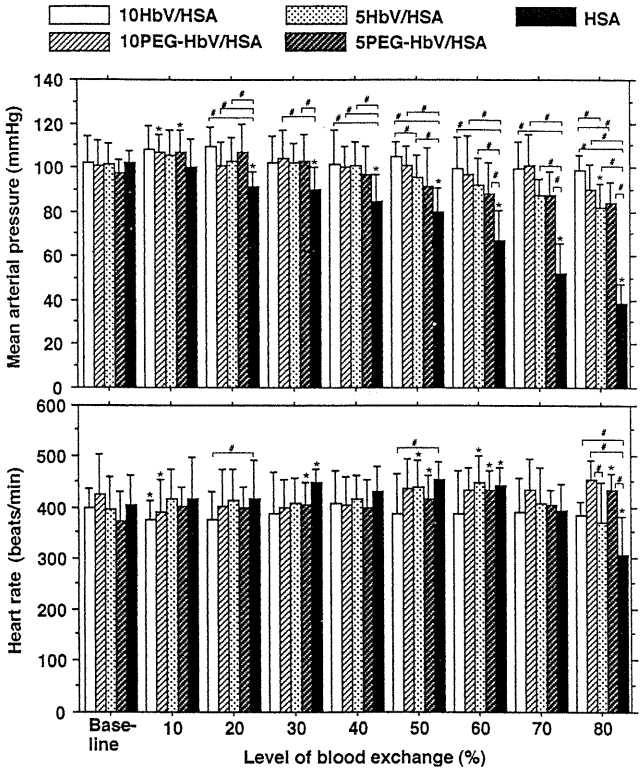

Figure 3. Changes in mean arterial pressure (top) and heart rate (bottom) during hemodilution. Values are mean ± SD. *Significantly different from baseline ($p < 0.05$); #significantly different between the indicated groups ($p < 0.05$).

groups to increase their visual contrast as the exchange progressed. This occurred even though the number of red cells decreased in comparison with control owing to the homogeneous dispersion of PEG-HbV in plasma phase as shown in Figure 4(b). Individual vesicles could not be seen at the magnification employed because the vesicle size was only 259 ± 82 nm. PEG-HbV was in the plasmatic gap between the RBC and endothelial cells, and also between the RBCs. Aggregates of the unmodified HbV were clearly observed in capillaries and venules where the flow rates were low [Fig. 4(c–e)]. The aggregates followed the red cells passing through the capillaries. Unmodified HbV aggregates appeared to flow in the capillaries centerline, which effectively "cleared" the capillary lumen of the vesicles. They formed large blocks or strings of aggregates in venules. *In vitro* experiments confirmed that the formation of aggregates was reversible and dependent on shear rate; however, they did not deform when the flow and shear rates were significantly lowered. The aggregate may also be present near the centerline of arteries, where shear stress was relatively small, compared with the proximity to the vascular wall, where shear stress was high.

Microhemodynamic results

The basal values for the microvessel diameters and blood flow rates are shown in Table III. There was no significant difference between the groups.

The HSA group at 60% or 80% exchange showed the most remarkable vasoconstrictions of A1 (–23% on average in comparison with baseline), A2 (–31%), and A3 (–26%) (Fig. 5). Both the 5 and 10 HbV/HSA groups, especially the former, showed a slight vasoconstriction of A1 and A2. There was no consistent trend in venules. The 10 HbV/HSA group showed the least changes in diameter or vasodilation in A3, A4, and Vc, while other groups tended to slightly vasoconstrict.

At 30% exchange, the HSA group had higher rates of blood flow by comparison with baseline in A2 (+57%), A3 (+8%), A4 (+27%), and Vc (+78%) (Fig. 6). This was a typical phenomenon for hemodilution with plasma expanders. However, the HSA group had a significant drop at the final exchange. Although the flow rates for HSA group in A3 and A4 were not calculated because of lack of resolution of the diameters of the arterioles owing to edema and decreased hematocrit, RBC velocity measured by the cross-correlation technique was significantly low in relation to other arterioles. All HbV/HSA and PEG-HbV/HSA groups showed significantly decreased blood flow; however, the PEG-HbV/HSA groups tended to maintain higher flow rates in comparison with unmodified HbV/HSA groups. Only the 5 PEG-HbV/HSA group showed a maximum rate in A3, which was the same as the HSA group. The 5 and 10 PEG-HbV/HSA groups showed comparably high blood flows even though the former had only half oxygen capacity, and were significantly higher than the HbV/HSA groups. The 5 HbV/HSA group showed a slightly improved perfusion to the 10 HbV/HSA. The flow rates of Vl were not necessarily related to other microvessels in the observed area, since Vl maintained with blood flow continued flowing even after A1 flow was stopped.

All groups maintained high functional capillary densities up to 60% exchange (Fig. 7). The HSA group showed the highest value up to 60% exchange; however, it dropped to the lowest (4.2 ± 10.2%) at 80% exchange. This result was in part related to blood flow velocity. The 5 and 10 PEG-HbV/HSA groups showed higher values (59.5 ± 27.3% and 42.1 ± 17.1%, respectively) compared to the unmodified HbV/HSA groups. Moreover, semitransparent elements (probably vesicles) were visible in capillaries of the PEG-HbV/HSA groups, even when there were no RBCs. Since functional capillary density was measured by counting the number of capillaries where RBCs were flowing, the values for the PEG-HbV/HSA groups might be underestimated.

TABLE II
Systemic Hematocrit and Blood Gas Parameters during Hemodilution

Group	Level of Blood Exchange			
	Baseline	30%	60%	80%
Systemic hematocrit (%)				
10 HbV/HSA	46.0 ± 3.1	32.7 ± 1.7*	17.7 ± 2.0*	7.3 ± 1.4*
10 PEG-HbV/HSA	45.1 ± 2.5	31.7 ± 4.1*	17.1 ± 1.6*	7.1 ± 1.6*
5 HbV/HSA	44.3 ± 3.8	32.0 ± 2.0*	17.5 ± 1.0*	7.0 ± 0.7*
5 PEG-HbV/HSA	45.0 ± 3.0	32.3 ± 3.2*	17.8 ± 1.0*	7.0 ± 2.2*
HSA	46.1 ± 3.4	31.1 ± 3.5*	16.4 ± 1.6*	6.5 ± 1.4*
P_aO_2 (mm Hg)				
10 HbV/HSA	58.1 ± 10.4	66.1 ± 10.4	67.0 ± 9.1†	64.8 ± 12.2†
10 PEG-HbV/HSA	62.3 ± 4.6	60.5 ± 8.7	58.4 ± 7.6†	62.3 ± 6.9†
5 HbV/HSA	57.8 ± 8.8	61.8 ± 12.1	68.7 ± 12.3†	67.8 ± 11.3†
5 PEG-HbV/HSA	58.8 ± 6.7	56.7 ± 3.6	66.5 ± 10.1†	65.3 ± 7.2†
HSA	58.9 ± 9.3	65.5 ± 10.4	92.4 ± 20.7*	108.0 ± 19.7*
P_aCO_2 (mm Hg)				
10 HbV/HSA	58.4 ± 6.5	57.1 ± 9.0	53.2 ± 7.4	49.4 ± 14.0
10 PEG-HbV/HSA	61.0 ± 6.7	61.3 ± 11.3	60.1 ± 7.4†	52.4 ± 4.2*†
5 HbV/HSA	59.6 ± 10.1	59.7 ± 11.3	54.8 ± 13.8	52.5 ± 11.0†
5 PEG-HbV/HSA	61.2 ± 4.7	58.8 ± 9.4	49.0 ± 6.4*	48.8 ± 8.2*
HSA	59.3 ± 11.6	57.0 ± 9.2	46.4 ± 10.8*	37.2 ± 13.6*
pH				
10 HbV/HSA	7.331 ± 0.038	7.327 ± 0.036	7.302 ± 0.041†	7.298 ± 0.034†
10 PEG-HbV/HSA	7.334 ± 0.024	7.315 ± 0.039	7.303 ± 0.021†	7.333 ± 0.034
5 HbV/HSA	7.323 ± 0.049	7.340 ± 0.046*	7.342 ± 0.064	7.323 ± 0.062
5 PEG-HbV/HSA	7.323 ± 0.027	7.325 ± 0.065	7.365 ± 0.047	7.352 ± 0.047
HSA	7.352 ± 0.065	7.351 ± 0.057	7.371 ± 0.082	7.392 ± 0.105
Base excess (mmol/L)				
10 HbV/HSA	6.07 ± 3.59	5.05 ± 2.99	1.70 ± 2.67	0.60 ± 2.80*†
10 PEG-HbV/HSA	3.64 ± 1.65	3.44 ± 1.52	1.74 ± 2.16	1.70 ± 1.41†
5 HbV/HSA	4.45 ± 2.98	5.95 ± 3.53	3.52 ± 2.76	1.23 ± 2.86*†
5 PEG-HbV/HSA	3.52 ± 3.22	3.68 ± 3.57	3.00 ± 2.93	1.65 ± 2.24†
HSA	6.59 ± 3.91	5.67 ± 1.50	2.90 ± 3.17	−3.78 ± 4.37*

Values are mean ± SD.
*Significant difference from baseline ($p < 0.05$).
†Significant difference from the HSA group ($p < 0.05$).
P_aO_2 = arterial blood oxygen tension; P_aCO_2 = arterial blood carbon dioxide tension.

stable values throughout hemodilution, while 10 PEG-HbV/HSA tended to increase with a maximum of 456 ± 37 beats/min at 80% exchange (baseline 425 ± 80 beats/min). The 5 HbV/HSA and 5 PEG-HbV/HSA groups had a maximum at 60% exchange (449 ± 53 and 435 ± 38 beats/min, respectively; baseline 398 ± 62 and 373 ± 58 beats/min, respectively). At 80% exchange, both PEG-HbV/HSA groups had higher values than the unmodified HbV/HSA groups.

In terms of blood gas parameters (Table II), the HSA group showed a P_aO_2 increase from 58.9 ± 9.3 mm Hg at baseline to 108.0 ± 19.7 mm Hg at 80% exchange, while P_aCO_2 decreased from 59.3 ± 11.6 to 37.2 ± 13.6 mm Hg owing to hyperventilation, a compensatory mechanism of anemia. All HbV/HSA and PEG-HbV/HSA groups showed more stable values than the HSA group. The pH value for the HSA group tended to increase slightly owing to respiratory alkalosis. The HSA group had the lowest base excess, −3.78 ± 4.37 mmol/L at 80% exchange (baseline 6.59 ± 3.91 mmol/L), indicating severe anemia. All HbV/HSA and PEG-HbV/HSA had rather stable values even after the exchange, although the unmodified 10 HbV/HSA group exhibited a slight decrease in both pH and base excess, while the unmodified 5 HbV/HSA only decreased base excess.

Flow patterns in microvasculature after hemodilution

Illumination with a blue light caused the inside of microvessels and capillaries of the PEG-HbV/HSA

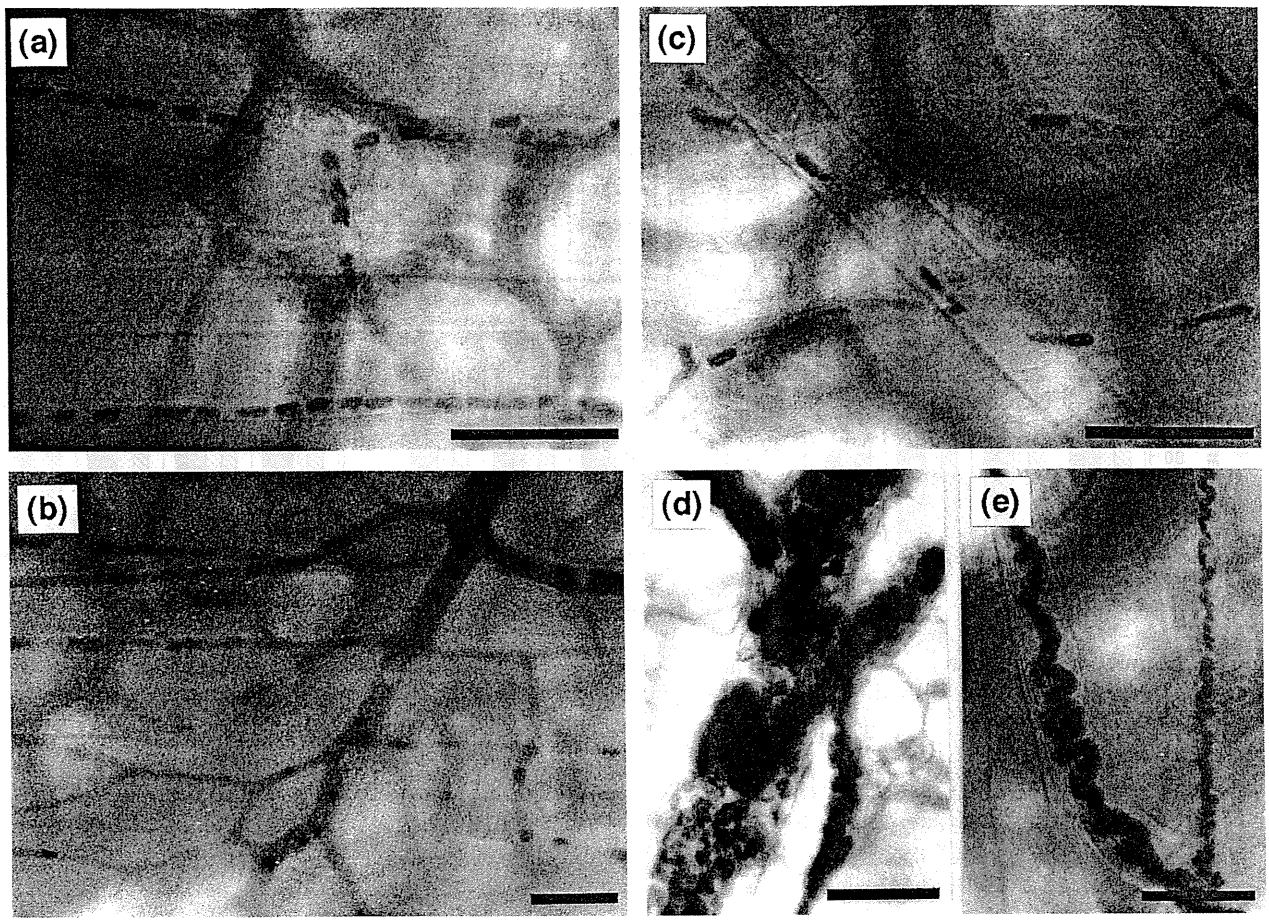

Figure 4. Micrographs of microvasculature (a) at normal condition, and at 80% exchange with (b) 10 PEG-HbV/HSA and (c–e) 10 HbV/HSA. A high contrast was obtained by illumination with a wavelength range of around 420 nm, being adsorbed at the Soret band of an Hb molecule. The bars indicate 50 μm. (a) Capillaries in normal condition where each RBC flows separately with a parachute-like configuration. The shape of vasculature is not clear. (b) The microvasculature of postcapillaries are blackened owing to the homogeneous dispersion of PEG-HbV particles in the plasma phase. (c) The aggregates of HbV are flowing after an RBC in capillaries. (d,e) The aggregates of HbV form blocks and chains in collecting venules.

Normally A1 had 45.5 ± 6.0 mm Hg in P_{O_2}, decreasing to 33.6 ± 8.7 mm Hg in A4 arterioles (Fig. 8). This reduction was associated with the diffusion of oxygen from these arterioles. After perfusion through the capillaries, the P_{O_2} in venules increased from 26.9 ± 10.2 mm Hg in Vc to 29.2 ± 7.8 mm Hg in Vl owing to the presence of an O_2 shunt. The P_{O_2} values of all groups after the completion of exchange were significantly

TABLE III
Basal Values for Diameters and Blood Flow Rates of Arterioles (A1–A4) and Venules (Vc and Vl)

Group	A1	A2	A3	A4	Vc	Vl
Diameter (μm)						
10 HbV/HSA	50.8 ± 11.9	25.0 ± 5.1	11.1 ± 3.6	7.7 ± 1.9	34.0 ± 9.6	95.8 ± 11.2
10 PEG-HbV/HSA	55.4 ± 15.5	25.9 ± 5.6	10.2 ± 3.1	9.1 ± 1.8	30.8 ± 5.1	94.1 ± 26.7
5 HbV/HSA	49.7 ± 10.5	24.6 ± 5.0	10.6 ± 2.8	8.9 ± 1.1	28.2 ± 2.7	82.9 ± 14.1
5 PEG-HbV/HSA	50.1 ± 13.8	23.0 ± 3.4	9.6 ± 3.0	9.8 ± 3.2	25.7 ± 9.2	91.0 ± 29.7
HSA	52.3 ± 13.3	26.0 ± 7.5	9.9 ± 2.9	7.2 ± 2.4	30.9 ± 7.6	104.0 ± 23.9
Blood flow rate (nL/s)						
10 HbV/HSA	4.29 ± 4.33	0.63 ± 0.55	0.13 ± 0.15	0.04 ± 0.05	0.11 ± 0.08	8.43 ± 5.83
10 PEG-HbV/HSA	5.17 ± 4.81	1.15 ± 0.67	0.33 ± 0.31	0.16 ± 0.19	0.24 ± 0.17	7.44 ± 4.89
5 HbV/HSA	4.06 ± 3.16	0.76 ± 0.63	0.17 ± 0.21	0.08 ± 0.09	0.07 ± 0.07	3.25 ± 0.62
5 PEG-HbV/HSA	5.46 ± 5.30	1.03 ± 1.13	0.19 ± 0.29	0.19 ± 0.27	0.14 ± 0.12	6.60 ± 8.33
HSA	5.50 ± 3.55	0.76 ± 0.49	0.17 ± 0.17	0.05 ± 0.05	0.17 ± 0.23	9.52 ± 3.32

Values are mean ± SD.

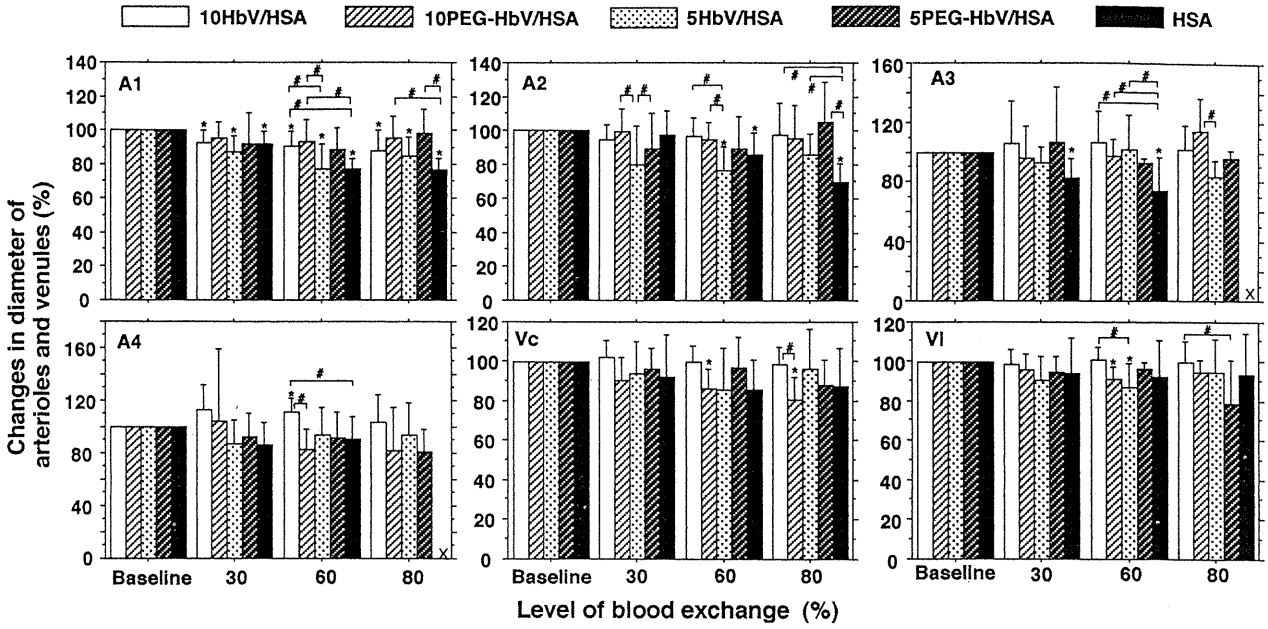

Figure 5. Diameter changes of arterioles (A1–A4) and venules (Vc and Vl) of the skinfold preparation during hemodilution. Values are mean ± SD. *Significantly different from baseline ($p < 0.05$); #significantly different between the indicated groups ($p < 0.05$). X = not measured.

lower than the baseline values. Among them, 10 PEG-HbV/HSA showed the highest values in all the microvessels. Even though there was a large difference in A1 Po_2 between the 10 PEG-HbV/HSA and HSA groups (about 70% and 10%, respectively, of the baseline value), the difference in interstitial Po_2 was small (about 3% and 2%, respectively). However, O_2 extraction (A1, interstitium) for the 10 PEG-HbV/HSA was similar to the baseline. Ranking of the Po_2 values was 10 PEG-HbV/HSA > 5 PEG-HbV/HSA > 5 HbV/HSA > 10 HbV/HSA > HSA.

DISCUSSION

Our results showed that PEG modification of the HbV surface significantly improved the performance

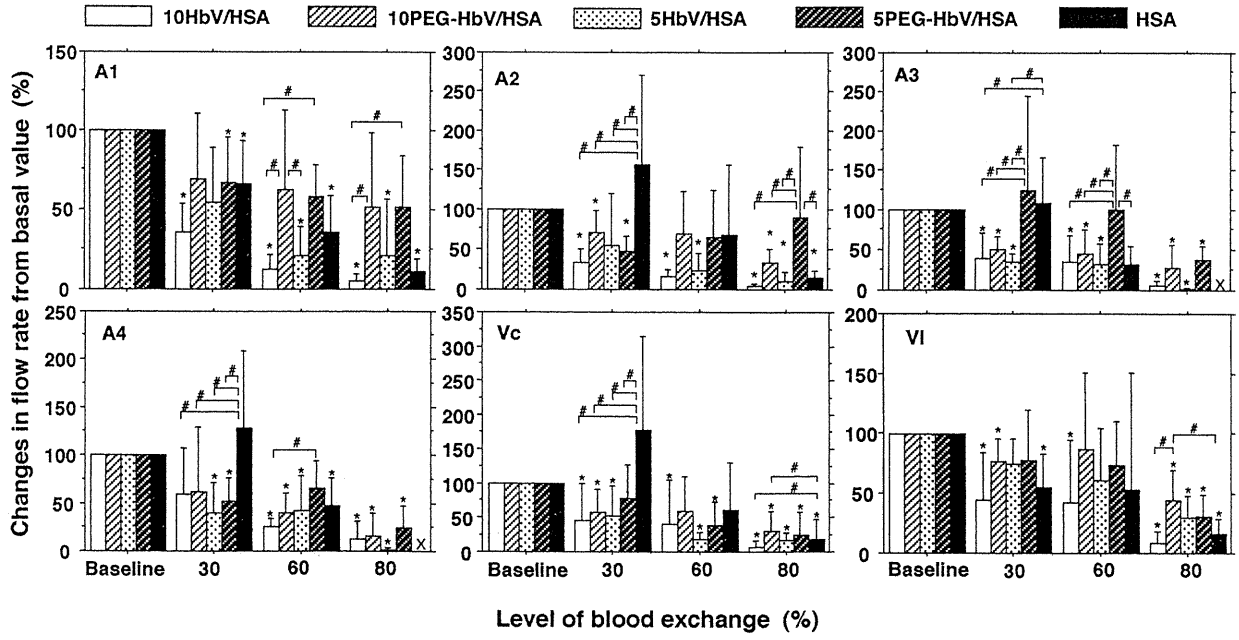

Figure 6. Changes in flow rates in arterioles (A1–A4) and venules (Vc and Vl) of the skinfold preparation during hemodilution. Values are mean ± SD. *Significantly different from baseline ($p < 0.05$); #significantly different between the indicated groups ($p < 0.05$). X = not measured owing to lack of diameter values; however, the RBC velocity was close to zero.

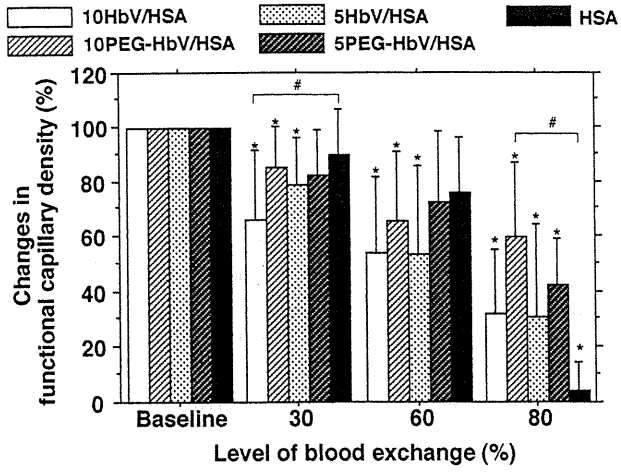

Figure 7. Changes in functional capillary density during hemodilution. Values are mean ± SD. *Significantly different from baseline ($p < 0.05$); #significantly different between the indicated groups ($p < 0.05$).

of HbV in the subcutaneous microcirculation. This result was not evident from analysis of systemic parameters which showed stable systemic hemodynamic conditions (Fig. 3) and blood gas parameters (Table II) for both PEG-modified and unmodified groups, but became apparent when analyzing corresponding microvascular responses to severe hemodilution of more than 80% hematocrit reduction. This level of hemodilution was necessary for safety and efficacy testing of Hb-based red cell substitute because up to 60% exchange, the HSA group yielded comparable blood flow rates and functional capillary density.

Blood flow rates for the HSA group showed a significant increase at 30% exchange for A2, A3, and A4 arterioles and Vc venules (Fig. 6). This flow increase

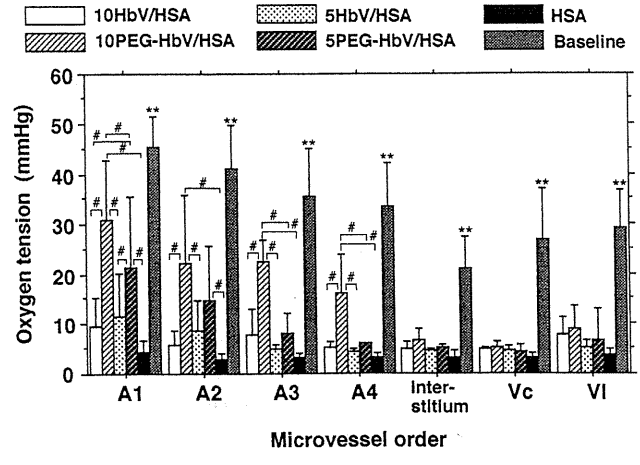

Figure 8. Oxygen tensions of microvasculature (A1–A4, Vc, and Vl) and interstitium after 80% exchange and baseline value. Values are mean ± SD. #Significant differences between the indicated groups ($p < 0.05$); **the baseline group showed significantly higher values than the other five groups ($p < 0.05$).

was related to the increase in cardiac output supposedly from an increase in heart rate (Fig. 3) compensating the decreased oxygen capacity and lower blood viscosity, a typical profile for hemodilution with a plasma expander observed in the same setting.[27] On the other hand, A1 and Vl did not show an increase, probably because they arcade, as evidenced by changes in flow direction, while other vessels always had one-way flow. The same trend was seen in the results of Lipowsky and Firrell,[37] where larger arterioles exhibited monotonous fall in flow with hemodilution, whereas increases in flow rate were found in smaller arterioles in cat mesenteric microvasculature. Flow in the HSA group eventually dropped as exchange progressed, and showed the lowest value at 80% exchange in relation to a decrease in heart rate and vasoconstriction. As whole-body oxygen delivery diminished, the fraction of cardiac output distributed to dermal, renal, and splanchnic beds declined, while the fraction redistributed to brain and myocardium should be maintained.[38,39]

The unmodified HbV/HSA groups monotonously decreased flow rate with the level of exchange, while the PEG-HbV/HSA groups maintained higher values even after completion of exchange (Fig. 6). This significant difference between the PEG-HbV and HbV groups was not related to the stable MAP and heart rates of both groups. This can be partly explained by the report of Chen et al. on the effect of hyperviscosity on regional hemodynamics,[40] in which the blood pressure and heart rate were stable even though viscosity was raised 2.4 times by the addition of high-molecular-weight dextran. In this study, there was significant redistribution of regional blood flow which was relatively constant in brain, but reduced in the small intestine, spleen, and thyroid (blood flow in the skin was not reported). It would appear that the large difference in viscosity between HbV/HSA (8 cP at 358 s^{-1}) and PEG-HbV/HSA (3.5 cP) in Figure 2 affects subcutaneous blood distribution in the same way. Contrary to expectation, 5 HbV/HSA, whose viscosity is half of 10 HbV/HSA, did not show a significant improvement. Aggregated HbV, present in the microvasculature (Fig. 4), may increase peripheral vascular resistance and adversely affect capillary perfusion. Even though it was confirmed *in vitro* that the aggregates dissociated reversibly at higher shear rates,[15] it is unlikely that they would dissociate in vessels where the flow rate or shear stress was low. Aggregation and decreased flow rate may constitute a vicious circle that reinforces negative effects on blood flow. The 5 PEG-HbV/HSA group showed compensatory flow increase in A3 owing to decreases in oxygen capacity and viscosity.

Microvascular Po_2 under normal conditions showed a gradient in the arterioles from the larger A1 to terminal arteriole A4, and then to collecting venules Vc

and large venule Vl. A slight increase in venules was due to a shunt. Normally, interstitial P_{O_2} was below that of A4. The difference between A1 and Vl was related to oxygen extraction and oxygen consumption in the area. After the 80% exchange with HSA, the gradient of P_{O_2} could hardly be observed and the microvasculature was hypoxic. The significant dissociation between markedly increased systemic P_aO_2 and microvascular P_{O_2} levels for the HSA group was due to compensatory pulmonary hyperventilation and significant reduction in blood flow in all microvessels. Arteriolar oxygen diffusion had been shown to play a key role in oxygenation under normal conditions.[19,41,42] Most of the physically dissolved oxygen in the plasma phase had already diffused out before blood arrived to the points of observation. The unmodified HbV/HSA groups were close to the HSA groups. The unmodified HbV/HSA exhibited higher viscosity owing to the formation of aggregates which may hinder capillary perfusion as shown in the micrograph (Fig. 4), leading to lower perfusion and lower interstitial P_{O_2}. On the other hand, the PEG-HbV/HSA groups showed a significant higher oxygenation. Even though microvascular P_{O_2} values were about 20–50% lower than control and interstitial P_{O_2} was slightly higher than that of the HSA group, the gradient appeared to parallel that of the control group. Oxygen consumption may be maintained to some extent with the aid of higher oxygen extraction by a decreased mixed venous P_{O_2} related to the decrease in Vl P_{O_2}. The 5 PEG-HbV/HSA group was significantly lower than the 10 PEG-HbV/HSA group even though blood flow rates and functional capillary density were comparable. This was probably due to the substantially lower Hb concentration and resulting lower oxygen capacity of 5 PEG-HbV/HSA than those of 10 PEG-HbV/HSA.

There was no vasoconstriction observed for the 10 PEG-HbV/HSA group. Administration of acellular Hb solutions showed a pressor effect. Hb had a high affinity of nitric oxide (NO) where binding induced vasoconstriction and hypertension. Previous studies of response to injections of αα-crosslinked Hb[22] and nitric oxide blockade (L-NMMA)[25] into conscious hamsters in the same experimental setting showed significant constriction in the same orders of arterioles. Vasoconstriction in the HbV/HSA groups and 5 PEG-HbV/HSA group was minimal compared with those experiments. Inhibition of NO–Hb binding related vasoconstriction for HbV had already been demonstrated by *in vitro* analysis of contractility of stripped aortic rings.[4,43] The present *in vivo* experiment confirmed that encapsulation of Hb inhibited NO-related vasoconstriction. The HSA group showed a slight vasoconstriction; however, it was due to the decreased MAP and blood supply to the subcutis. The 10 HbV/HSA group tended to dilate the Vc and Vl, probably because the aggregated HbV, which did not dissociate, tended to stay in the venules.

Both PEG-HbV and unmodified HbV groups showed a slight increase in MAP as the fluids were injected (10% exchange) (Fig. 3). However, this was not necessarily accompanied by vasoconstriction (Fig. 5). This level of hypertension was quite small in comparison with the acellular Hb injection.[6,7] The same transient subtle increase in blood pressure was confirmed when HbV was infused into anesthetized Wistar rats; this was attributed to anaphylactic reactions related to phospholipid vesicle injection, and not to the presence of Hb.[3,15,44,45] A transient thrombocytopenia was observed and the platelets accumulated in sheep lung.[46] There was a possibility that the same reaction was present in hamsters. These effects notwithstanding, MAP for both PEG-HbV and unmodified HbV maintained normal values even after the completion of blood substitution, which cannot be achieved by HSA alone.

Our results showed that both PEG-modified and unmodified HbV maintained systemic parameters at normal levels, while PEG-HbV yielded a significant improvement in subcutaneous microcirculation as evidenced by RBC velocity, functional capillary density, and microvascular P_{O_2}. These results highlighted the importance of inhibition of intervesicular aggregation for vesicles encapsulating Hb, although many of the reported studies of this type of red cell substitute did not consider aggregation and its influences.[1,2,47] A previous study showed that PEG-HbV and HbV did not exhibit significant difference in interaction between vesicles and albumin,[15] and PEG chains should sterically prevent intervesicular access and aggregation rather than albumin adsorption.[48–50] Because PEG chains do not completely cover the surface of the vesicles at the molar composition employed, albumin could pass through the PEG chain layers and arrive at the vesicular surface to be adsorbed. Even so, repulsion between the PEG-modified vesicles, which were much larger than albumin, should be effective in preventing vesicular aggregation owing to adsorbed albumin on the surface. This hypothesis was also supported by the results of Harasym et al.,[51] who showed that coupling of avidin onto PEG-modified phospholipid vesicles was not retarded, but aggregation during coupling was suppressed by PEG chains. Steric hindrance was effective with larger proteins, vesicles, and RES. It was also possible that PEG modification suppressed interaction with endothelial cells on the vascular wall in the same manner. However, at present, we do not have the means to determine if PEG chains suppress side reactions with the vascular wall and improve microvascular perfusion.

The overall microvascular responses for the 10 PEG-HbV/HSA are still not fully satisfactory, since tissue oxygenation is deficient for all groups. It appears that

the subcutaneous blood supply is controlled by larger arteries closer to the heart. We speculate that this result could be related to a rheological effect and autoregulatory responses. Steric hindrance of PEG chains inhibits intervesicular access and aggregation; however, the resulting low viscosity associated with PEG-modified vesicles should cause a decrease in shear stress and consequent reduction in the release of endothelial relaxing factors,[52–54] inducing vasoconstriction in larger vessels closer to the heart, not evident in this preparation, and decreased microvascular blood flow and oxygen tension. These effects could, in part, be magnified by autoregulatory responses owing to greater availability of oxygen from vesicles compared to RBCs. Although oxygen affinity of both types of HbVs is nearly the same as for blood, HbVs show a faster oxygen uptake and release owing to the smaller particle size.[43,55] Paradoxically, high oxygen availability at the arteriolar level may engage a mechanism designed to maintain arteriolar P_{O_2} at a present level, a process leading to vasoconstriction superimposed on the responses to nonoptimal rheological properties.[19,56] This hypothesis is supported by the similarity in the microvascular blood flow of 5 PEG-HbV/HSA and 10 PEG-HbV/HSA exchanges, even though oxygen capacity is reduced.

In conclusion, PEG-modified HbV particles have been developed with stable and uniform characteristics that show improved microvascular responses to severe hemodilution compared with unmodified HbV and HSA alone. These results indicate a promising avenue for chemical modification of vesicles that may eventually lead to the formulation of an effective oxygen carrying blood replacement fluid consisting of the red cell substitute.

H.S. is an overseas research fellow of the Japan Society for the Promotion of Science. The authors thank Dr. T. Kose for technical cooperation.

References

1. L. Djordjevich, J. Mayoral, I. F. Miller, and A. D. Ivankovich, "Cardiorespiratory effects of exchange transfusions with synthetic erythrocytes in rats," *Crit. Care Med.*, **15**, 318–323 (1987).
2. C. A. Hunt, R. R. Burnette, R. D. MacGregor, A. E. Strubbe, T. D. Lau, N. Taylor, and H. Kawada, "Synthesis and evaluation of a prototypal artificial red cell," *Science*, **30**, 1165–1168 (1985).
3. A. S. Rudolph, "Encapsulation of hemoglobin in liposomes," in *Blood Substitutes: Physiological Basis of Efficacy*, R. M. Winslow, K. D. Vandegriff, and M. Intaglietta (eds.), Birkhäuser, Boston, 1995, pp. 90–104.
4. E. Tsuchida and S. Takeoka, "Stabilized hemoglobin vesicles," in *Artificial Red Cells*, E. Tsuchida (ed.), Wiley, New York, 1995, pp. 35–64.
5. R. M. Winslow, "Blood substitutes: A moving target," *Nat. Med.*, **1**, 1212–1215 (1995).
6. S. C. Schultz, B. Grady, F. Cole, I. Hamilton, K. Burhop, and D. S. Malcolm, "A role for endothelin and nitric oxide in the pressor response to diaspirin cross-linked hemoglobin," *J. Lab. Clin. Med.*, **122**, 301–308 (1993).
7. P. E. Keipert, A. Gonzales, G. L. Gomez, V. W. Macdonald, J. R. Hess, and R. M. Winslow, "Acute changes in systemic blood pressure and urine output of conscious rats following exchange transfusion with diaspirin-crosslinked hemoglobin solution," *Transfusion*, **33**, 701–708 (1993).
8. S. Moncada, R. M. J. Palmer, and E. A. Higgs, "Nitric oxide: Physiology, pasophysiology, and pharmacology," *Pharmacol. Rev.*, **43**, 109–142 (1991).
9. A. G. Tsai, H. Kerger, and M. Intaglietta, "Microvascular oxygen distribution: Effects due to free hemoglobin in plasma," in *Blood Substitutes: New Challenges*, R. M. Winslow, K. D. Vandegriff, and M. Intaglietta (eds.), Birkhäuser, Boston, 1996, pp. 124–131.
10. S. B. Olsen, D. B. Tang, M. R. Jackson, E. R. Gomez, B. Ayala, and B. M. Alving, "Enhancement of platelet deposition by cross-linked hemoglobin in a rat carotid endarterectomy model," *Circulation*, **93**, 327–332 (1996).
11. W. Kaca, R. I. Roth, K. D. Vandegriff, G. C. Chen, F. A. Kuypers, R. M. Winslow, and J. Levin, "Effects of bacterial endotoxin on human cross-linked and native hemoglobins," *Biochemistry*, **34**, 11176–11185 (1995).
12. A. L. Klibanov, K. Maruyama, and V. P. Torchilin, "Amphiphatic polyethyleneglycols effectively prolong the circulation time of liposomes," *FEBS Lett.*, **26**, 8235–8237 (1990).
13. M. C. Woodle and D.D. Lasic, "Sterically stabilized liposomes," *Biochim. Biophys. Acta*, **1113**, 171–199 (1992).
14. H. Yoshioka, "Surface modification of haemoglobin-containing liposomes with polyethylene glycol prevents liposome aggregation in blood plasma," *Biomaterials*, **12**, 861–864 (1991).
15. H. Sakai, S. Takeoka, S. I. Park, T. Kose, K. Hamada, Y. Izumi, A. Yoshizu, H. Nishide, K. Kobayashi, and E. Tsuchida, "Surface-modification of hemoglobin vesicles with polyethyleneglycol and effects on aggregation, viscosity, and blood flow during 90% exchange transfusion in anesthetized rats," *Bioconjugate Chem.*, **8**, 15–22 (1997).
16. S. Zheng, R. Beissinger, R. L. Sherwood, D. L. McCormick, D. D. Lasic, and F. J. Martin, "Liposome-encapsulated hemoglobin: a red blood cell substitute," *J. Liposome Res.*, **3**, 575–588 (1993).
17. A. Usuba and R. Motoki, "Safety and efficacy of encapsulated hemoglobin in hemorrhagic shock," in *Artificial Red Cells*, E. Tsuchida (ed.), Wiley, New York, 1995, pp. 65–92.
18. Y. Izumi, H. Sakai, K. Hamada, S. Takeoka, K. Yamahata, H. Katoh, H. Nishide, E. Tsuchida, and K. Kobayashi, "Physiological responses to exchange transfusion with hemoglobin vesicles as an artificial oxygen carrier in anesthetized rats: Changes in mean arterial pressure and renal cortical tissue oxygen tension," *Crit. Care Med.*, **24**, 1869–1873 (1996).
19. M. Intaglietta, P. C. Johnson, and R. M. Winslow, "Microvascular and tissue oxygen distribution," *Cardiovasc. Res.*, **32**, 632–643 (1996).
20. H. Kerger, A. G. Tsai, D. J. Saltzman, R. M. Winslow, and M. Intaglietta, "Fluid resuscitation with oxygen versus non-oxygen carriers after 2-hour hemorrhagic shock in conscious hamsters," *Am. J. Physiol.*, **272** (*Heart Circ. Physiol.* **41**), H525–H537 (1997).
21. H. Kerger, D. J. Saltzman, A. Gonzales, A. G. Tsai, K. van Ackern, R. M. Winslow, and M. Intaglietta, "Microvascular oxygen delivery and interstitial oxygenation during sodium pentobarbital anesthesia," *Anesthesiology*, **86**, 372–386 (1997).
22. A. G. Tsai, H. Kerger, and M. Intaglietta, "Microcirculatory consequences of blood substitution with αα-hemoglobin," in *Blood Substitutes: Physiological Basis of Efficacy*, R. M. Winslow,

K. D. Vandegriff, and M. Intaglietta (eds.), Birkhäuser, Boston, 1995, pp. 155–174.

23. H. Kerger, D. J. Saltzman, M. D. Menger, K. Messmer, and M. Intaglietta, "Systemic and subcutaneous microvascular oxygen tension dissociation during 4-hour hemorrhagic shock in conscious hamsters," *Am. J. Physiol.*, **270** (*Heart Circ. Physiol.* **39**), H827–H836 (1996).
24. H. Kerger, I. P. Torres Filho, M. Rivas, R. M. Winslow, and M. Intaglietta, "Systemic and subcutaneous microvascular oxygen tension in conscious Syrian golden hamsters," *Am. J. Physiol.*, **267** (*Heart Circ. Physiol.*, **37**), H802–H810 (1995).
25. S. Bertuglia, A. Colantuoni, and M. Intaglietta, "Effects of L-NMMA and indomethacin on arteriolar vasomotion in skeletal muscle circulation of conscious and anesthetized hamsters," *Microvasc. Res.*, **48**, 68–84 (1994).
26. I. P. Torres Filho and M. Intaglietta, "Microvascular Po_2 measurements by phosphorescence decay method," *Am. J. Physiol.*, **265** (*Heart Circ. Physiol.* **34**), H1434–H1438 (1993).
27. S. Mirhashemi, G. A. Breit, R. H. Chavez Chavez, and M. Intaglietta, "Effects of hemodilution on skin microcirculation," *Am. J. Physiol.*, **254** (*Heart Circ. Physiol.* **23**), H411–H416 (1988).
28. H. D. Papenfuss, J. F. Gross, M. Intaglietta, and F. A. Treese, "A transparent access chamber for the rat dorsal skin fold," *Microvasc. Res.*, **18**, 311–318 (1979).
29. H. Sakai, S. Takeoka, H. Yokohama, Y. Seino, H. Nishide, and E. Tsuchida, "Purification of concentrated hemoglobin using organic solvent and heat treatment," *Protein Express. Purif.*, **4**, 563–569 (1993).
30. H. Sakai, K. Hamada, S. Takeoka, H. Nishide, and E. Tsuchida, "Physical characteristics of hemoglobin vesicles as red cell substitutes," *Biotechnol. Progress*, **12**, 119–125 (1996).
31. J. E. Chung, K. Hamada, H. Sakai, S. Takeoka, and E. Tsuchida, "Ligand exchange reaction of carbonylhemoglobin to oxyhemoglobin in a hemoglobin liquid membrane," *Nippon Kagaku Kaishi*, **2**, 123–127 (1995).
32. M. Intaglietta and W. R. Tompkins, "Microvascular measurements by video image shearing and splitting," *Microvasc. Res.*, **5**, 309–312 (1973).
33. M. Intaglietta, N. R. Silverman, and W. R. Tompkins, "Capillary flow velocity measurements in vivo and in situ by television methods," *Microvasc. Res.*, **10**, 165–179 (1975).
34. H. Lipowsky and B. Zweifach, "Application of the 'two-slit' photometric technique to the measurement of microvascular volumetric flow rates," *Microvasc. Res.*, **15**, 93–101 (1978).
35. A. R. de Gandio, "Therapeutic use of albumin," *Int. J. Artif. Organs*, **18**, 216–224 (1995).
36. W. L. Rumsey, J. M. Vandercooi, and D. F. Wilson, "Imaging of phosphorescence: A novel method for measuring oxygen distribution in perfused tissue," *Science*, **241**, 1649–1651 (1988).
37. H. H. Lipowsky and J. C. Firrell, "Microvascular hemodynamics during systemic hemodilution and hemoconcentration," *Am. J. Physiol.*, **250** (*Heart Circ. Physiol.* **19**), H908–H922 (1988).
38. R. Schlichtig, D. J. Kramer, and M. R. Pinsky, "Flow redistribution during progressive hemorrhage is a determinant of a critical O_2 delivery," *J. Appl. Physiol.*, **70**, 169–178 (1991).
39. R. C. Koehler, R. J. Traystman, and M. D. Johnes, Jr., "Regional blood flow and O_2 transport during hypoxic and CO hypoxia in neonatal and adult sheep," *Am. J. Physiol.*, **248** (*Heart Circ. Physiol.* **17**), H118–H124 (1985).
40. R. Y. Z. Chen, R. D. Carlin, S. Simchon, K. M. Jan, and S. Chien, "Effects of dextran-induced hyperviscosity on regional blood flow and hemodynamics in dogs," *Am. J. Physiol.*, **256** (*Heart Circ. Physiol.* **25**), H898–H905 (1989).
41. D. P. Swain and R. N. Pittman, "Oxygen exchange in the microcirculation of hamster retractor muscle," *Am. J. Physiol.*, **256** (*Heart Circ. Physiol.* **25**), H247–H255 (1989).
42. M. L. Ellsworth and R. N. Pittman, "Arterioles supply oxygen to capillaries by diffusion as well as convection," *Am. J. Physiol.*, **258** (*Heart Circ. Physiol.* **27**), H1240–H1243 (1990).
43. K. Nakai, T. Ohta, I. Sakuma, K. Akama, Y. Kobayashi, S. Tokuyama, A. Kitabatake, Y. Nakazato, T. A. Takahashi, and S. Sekiguchi, "Inhibition of endothelium-dependent relaxation by hemoglobin in rabbit aortic strips: Comparison between acellular hemoglobin derivatives and cellular hemoglobins," *J. Cardiovasc. Pharmacol.*, **28**, 115–123 (1996).
44. H. C. Loughley, M. B. Bally, L. W. Reihish, and P. R. Cullis, "The binding of phosphatidylglycerol liposomes to rat platelets is mediated by complement," *Thromb. Haemostas.*, **64**, 172–176 (1990).
45. M. Watanabe, H. Ohyanagi, and Y. Saitoh, "Experimental study on anaphylactic effects by fluosol DA as an oxygen carrier," *Jpn. J. Artif. Organs*, **17**, 1513–1522 (1988).
46. K. Miyamoto, E. Schultz, T. Heath, M. D. Mitchell, K. H. Albertine, and N. C. Staub, "Pulmonary intravascular macrophages and hemodynamic effects of liposomes in sheep," *J. Appl. Physiol.*, **64**, 1143–1152 (1988).
47. R. Rabinovici, A. S. Rudolph, J. Vernick, and G. Feuerstein, "Lyophilized liposome encapsulated hemoglobin: evaluation of hemodynamic, biochemical, and hematologic responses," *Crit. Care Med.*, **22**, 480–485 (1994).
48. A. Klibanov, K. Maruyama, A. M. Beckerleg, V. P. Torchilin, and L. Huang, "Activity of amphipathic poly(ethylene glycol) 5000 to prolong the circulation time of liposomes depends on the liposome size and its unfavorable for immunoliposome binding to target," *Biochim. Biophys. Acta*, **1062**, 142–148 (1991).
49. D. Needham, T. J. McIntosh, and D. D. Lasic, "Repulsive interactions and mechanical stability of polymer-grafted lipid membranes," *Biochim. Biophys. Acta*, **1108**, 40–48 (1992).
50. V. P. Torchilin, V. G. Omelyaneko, M. I. Papisov, A. A. Bogdanov, Jr., V. S. Trubetskoy, J. N. Herron, and C. A. Gentry, "Poly(ethylene glycol) on the liposome surface: On the mechanism of polymer-coated liposome longevity," *Biochim. Biophys. Acta*, **1195**, 11–20 (1994).
51. T. O. Harasym, P. Tardi, S. A. Longman, S. M. Ansell, M. B. Bally, R. P. Cullis, and L. S. Choi, "Poly(ethylene glycol)-modified phospholipid prevent aggregation during covalent conjugation of proteins to liposomes," *Bioconjugate Chem.*, **6**, 187–194 (1995).
52. A. M. Malek and S. Izumo, "Control of endothelial cell gene expression by flow," *J. Biomech.* **28**, 1515–1528 (1995).
53. A. Koller, D. Sun, and G. Kaley, "Role of shear stress and endothelial prostaglandins in flow- and viscosity-induced dilation of arterioles in vitro," *Circ. Res.*, **72**, 1276–1284 (1993).
54. V. Smiesko, D. J. Lang, and P.C. Johnson, "Dilator response of rat mesenteric arcading arterioles to increased blood flow velocity," *Am. J. Physiol.*, **257** (*Heart Circ. Physiol.* **26**), H1958–H1965 (1989).
55. K. D. Vandegriff and J. S. Olson, "Morphological and physiological factors affecting oxygen uptake and release by red blood cells," *J. Biol. Chem.*, **259**, 12619–12627 (1984).
56. P. C. Johnson, K. Richmond, R. D. Shonat, A. Toth, M. Pal, M. E. Tischler, and R. M. Lynch, "Oxygen delivery regulation: Implications for blood substitutes," in *Blood Substitutes: Physiological Basis of Efficacy*, R. M. Winslow, K. D. Vandegriff, and M. Intaglietta (eds.), Birkhäuser, Boston, 1995, pp. 175–186.

FARADAY

Physical properties and packing states of molecular assemblies of synthetic glycolipids in aqueous dispersions

Shinji Takeoka,[a] Keitaro Sou,[a] Christoph Boettcher,[b] Jürgen-Hinrich Fuhrhop[b] and Eishun Tsuchida[a]*

[a]*Department of Polymer Chemistry, Advanced Research Institute for Science and Engineering, Waseda University, Tokyo 169-8555, Japan*

[b]*Institute für Organische Chemie, Freie Universität Berlin, Takustraße 3, 14195 Berlin*

Amidic glycolipids, 1,5-bis-*O*-alkyl-*N*-maltooligonoyl-L-glutamate (**1**), having various lengths of two hydrocarbon chains (carbon number, *m*: 14, 16, 18) and maltooligotose with (glucose unit, *n*: 3, 5, 7) and a *N*-glycosidic lipid, 1,5-bis-*O*-octadecyl-*N*-maltopentaonosyl-L-glutamate (**2**) have been synthesized. The assembling structures were analyzed by microscopic observation, such as negatively stained TEM, cryo-TEM, and AFM. The glycolipid **1a** (*m*,*n*: 14,5) showed a fiber-like structure in all the observed temperatures, while **1b** (16,5) showed a fiber-like structure when the hydrating temperature was above the gel-to-liquid crystalline phase transition temperature (T_c ; 45 °C) and a large disk-like structure when incubated below the T_c. The glycolipid **1c** (18,5) took a large disk-like structure after hydration of the powder above the T_c. The glycolipids **1d** (18,3) and **1e** (18,7) showed a mixture of large disks and large vesicles and a mixture of small disks and micelles, respectively. The *N*-glycosidic lipid, **2**, with no amide linkage made a vesicular structure only. The preparation procedure using high shear stress, such as extrusion and sonication, converted the large disk of **1c** to smaller assemblies, such as small disk-, cone-, and granule-like assemblies, depending on the preparation conditions. The glycolipid molecules in the planer part of the disk were packed so tightly that molecular mobility was very low even above the T_c (58 °C), and the reactivity of the saccharide chain against Concanavalin A was also very low, indicating that the high reactivity probably comes from the loose packing of saccharide chains around the edge part of the assemblies.

Introduction

Saccharide chains of glycolipids and glycoproteins located on the outer surface of cells have important roles in the expression of biological messages, in cell identification, or triggers for various cascades, in antigen–antibody reactions, *etc.*[1–3] Recently, glyco-conjugated molecular biology and physiology have been extensively developed, and their important roles in living systems have been vigorously clarified.[3] Because most glycolipids consist of one saccharide chain and a spacer, and two alkyl chains, their molecular structures can be characterized from the saccharide chain length, the structure of the glucose unit, the binding of the saccharide chain, the kinds of spacer, the alkyl chain length, *etc.* Like the assemblies of phospholipids, the glycolipids assemble in various ways, depending on their hydrophilic–hydrophobic balance, stearic hindrance, the saccharide part interface, *etc.* The assembling states and structures of natural or synthetic glycolipids have been studied by Maggio and co-workers,[4–6] Hato and co-workers,[7,8] and others.[9–14] We have synthesized a series of simple glycolipids, of which the head-groups are maltooligotoses, and the hydrophobic part contains one or two alkyl chains.[15–17] We also clarified that phospholipid vesicles mixed with glycolipids show remarkable stabilities in an aqueous dispersion[15,16] or a frozen state.[17] Because the hydrophilic–hydrophobic balance of the glycolipids can be easily changed by changing the length of the saccharide chain or the alkyl chain without changing the basic structure,[7,8,12] glycolipids become useful molecules for studying the relationships between the molecular structure, the morphology of glycolipid assemblies, and their reactivities.

In this paper, the assembling structures of a series of glycolipids are studied in relation to the ratio of the saccharide part and the alkyl chain part, and to the strength of the energy applied in the preparation of the assemblies. The detailed molecular packing and thermodynamic properties of the various molecular assemblies are studied and discussed as well as the reactivity of the saccharide chains with recognition molecules such as Concanavalin A (Con A) in the various assemblies.

Syntheses

Syntheses of 1,5-bis-*O*-alkyl-*N*-maltooligonoyl-L-glutamates (1a–e)

Synthesis of maltopentaonolactone.[18] Maltopentaose (23.0 g, 27.8 mmol) was dissolved into pure water (460 ml) in the presence of calcium carbonate (6.7 g, 66.6 mmol). Bromine (8.8 g, 5.1 mmol) was added dropwise into the mixed solution. The mixture was stirred at 25 °C for 14 h. The reaction was monitored by silica gel thin-layer chromatography (silica gel 60 F_{254}, Merck). The calcium carbonate and calcium bromide were removed by filtration. Silver carbonate (18.0 g, 65.4 mmol) was added to the solution and the solution stirred at 25 °C for 2 h. The silver bromide and the remaining silver carbonate were removed by centrifugation (1600*g*, 10 min) and filtration. The calcium carboxylate obtained at the anomer position of maltopentaose was converted to an acid-form by a cation-exchange resin (Amberlite IR 120B). The solution was evaporated and dried at 80 °C for 30 h *in vacuo* to give a white solid of maltopentaonolactone (18.0 g, yield 78%).

Maltotrionolactone and maltoheptaonolactone were synthesized in the same way. Their yields were 81% and 80%, respectively.

Synthesis of 1,5-bis-*O*-[tetra(*n*-butylammonium)]-*N*-maltopentaonoyl-L-glutamate. Maltopentaonolactone (18.0 g, 21.8 mmol) and 1,5-bis-*O*-[tetra(*n*-butylammonium)]-L-glutamate (22.6 g, 35.9 mmol) were dissolved in DMF. The solution was

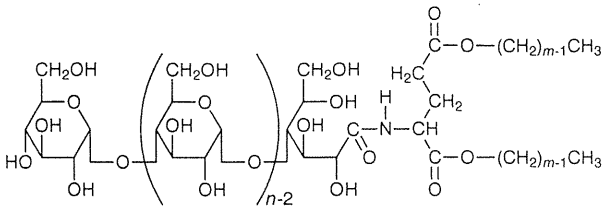

1a (m = 14, n = 5)
1b (m = 16, n = 5)
1c (m = 18, n = 5)
1d (m = 18, n = 3)
1e (m = 18, n = 7)

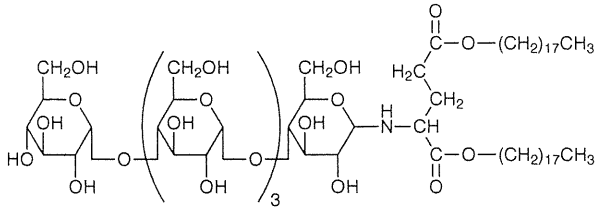

2

stirred at 70 °C for 16 h, and reprecipitated with acetone twice to give a light brown powder of 1,5-bis-*O*-[tetra(*n*-butylammonium)]-*N*-maltopentaonoyl-L-glutamate (28.0 g, yield 88%).

1,5-Bis-*O*-[tetra(*n*-butylammonium)]-*N*-maltotrionoyl-L-glutamate and 1,5-bis-*O*-[tetra(*n*-butylammonium)]-*N*-maltoheptaonoyl-L-glutamate were synthesized in the same way. Their yields were 80% and 82%, respectively.

Synthesis of 1,5-bis-*O*-octadecyl-*N*-maltopentaonoyl-L-glutamate [1c (18,5)]. Bromooctadecane (1.9 g, 5.7 mmol) and 1,5-bis-*O*-[tetra(*n*-butylammonium)]-*N*-maltopentaonoyl-L-glutamate (1.0 g, 0.7 mmol) were dissolved in DMF and stirred at 60 °C for 8 h. The reaction mixture was reprecipitated twice with acetone. The precipitate was recrystallized from mixed solvent ($CHCl_3/CH_3OH/H_2O$ = 3/4/1 v/v/v) at 4 °C to give 1,5-bis-*O*-octadecyl-*N*-maltopentaonoyl-L-glutamate (0.73 g, yield 71%) as a white powder. IR (KBr): 1736 cm^{-1} [ν(C=O)], 1655 cm^{-1} [ν(N—H)]; ^{1}H-NMR ([$^2H_6$]DMSO, 200 MHz): δ 0.8 (6H), 1.2 (60H), 1.5 (4H), 2.0 (2H), 2.3 (2H), 2.7– ≈ 6.0 (56H), 7.8 (1H).

1,5-Bis-*O*-tetradecyl-*N*-maltopentaonoyl-L-glutamate [**1a** (14,5)] and 1,5-bis-*O*-hexadecyl-*N*-maltopentaonoyl-L-glutamate [**1b** (16,5)] were synthesized in the same way. 1,5-Bis-*O*-tetradecyl-*N*-maltopentaonoyl-L-glutamate: (0.68 g, yield 50%); IR (KBr): 1736 cm^{-1} [ν(C=O)], 1655 cm^{-1} [ν(N—H)]; ^{1}H-NMR ([$^2H_6$]DMSO, 200 MHz): δ 0.8 (6H), 1.2 (44H), 1.5 (4H), 2.0 (2H), 2.3 (2H), 2.7– ≈ 6.0 (56H), 7.8 (1H). 1,5-Bis-*O*-hexadecyl-*N*-maltopentaonoyl-L-glutamate: (1.0 g, yield 50%); IR (KBr): 1736 cm^{-1} [ν(C=O)], 1655 cm^{-1} [ν(N—H)]; ^{1}H-NMR ([$^2H_6$]DMSO, 200 MHz): δ 0.8 (6H), 1.2 (52H), 1.5 (4H), 2.0 (2H), 2.3 (2H), 2.7– ≈ 6.0 (56H), 7.8 (1H).

Synthesis of 1,5-bis-*O*-octadecyl-*N*-maltotrionoyl-L-glutamate [1d (18,3)]. Bromooctadecane (1.5 g, 4.5 mmol) and 1,5-bis-*O*-[tetra(*n*-butylammonium)]-*N*-maltotrionoyl-L-glutamate (1.0 g, 0.9 mmol) were dissolved in DMF and stirred at 60 °C for 8 h. The reaction mixture was reprecipitated twice with acetone. The precipitate was recrystallized from a mixed solvent ($CHCl_3/CH_3OH$ = 5/3 v/v) at 4 °C to give 1,5-bis-*O*-octadecyl-*N*-maltotrionoyl-L-glutamate (0.79 g, yield 63%) as a white powder. IR (KBr): 1736 cm^{-1} [ν(C=O)], 1655 cm^{-1} [ν(N—H)]; ^{1}H-NMR ([$^2H_6$]DMSO, 200 MHz): δ 0.8 (6H), 1.2 (60H), 1.5 (4H), 2.0 (2H), 2.3 (2H), 2.7– ≈ 6.0 (36H), 7.8 (1H).

Synthesis of 1,5-bis-*O*-octadecyl-*N*-maltoheptaonoyl-L-glutamate [1e (18,7)]. Bromooctadecane (0.07 g, 0.2 mmol) and 1,5-bis-*O*-[tetra(*n*-butylammonium)]-*N*-maltopentaonoyl-L-glutamate (0.045 g, 0.025 mmol) were dissolved in DMF and stirred at 60 °C for 12 h. The reaction mixture was reprecipitated with acetone. The precipitate was purified by silica gel chromatography ($CHCl_3/CH_3OH/H_2O$ = 5/4/1 v/v/v) to give 1,5-bis-*O*-octadecyl-*N*-maltoheptaonoyl-L-glutamate (0.0054 g, yield 12%) as a white powder. IR (KBr): 1736 cm^{-1} [ν(C=O)], 1655 cm^{-1} [ν(N—H)]; ^{1}H-NMR ([$^2H_6$]DMSO, 200 MHz): δ 0.8 (6H), 1.2 (60H), 1.5 (4H), 2.0 (2H), 2.3 (2H), 2.7– ≈ 6.0 (76H), 7.8 (1H).

Synthesis of 1,5-bis-*O*-octadecyl-*N*-maltopentaonocyl-L-glutamate [2 (18,5)]

Glutamic acid (1.47 g, 10 mmol) and *p*-toluenesulfonic acid (2.28 g, 12 mmol) were dissolved in benzene and refluxed at 80 °C for 1 h. Stearyl alcohol (5.94 g, 22 mmol) was added into the solution and refluxed at 80 °C for 8 h for the removal of water. The reaction mixture was washed with saturated Na_2CO_3 aqueous solution, and benzene was evaporated off. The solid was recrystallized from methanol at 4 °C to give 1,5-bis-*O*-octadecyl-L-glutamate (5.09 g, yield 78%) as a white solid.

Maltopentaose (0.5 g, 0.6 mmol) and 1,5-bis-*O*-octadecyl-L-glutamate (0.5 g, 0.6 mmol) were dissolved in DMF and stirred at 80 °C for 6 h. The reaction mixture was reprecipitated with acetone, and the precipitate was washed with pure water to give 1,5-bis-*O*-octadecyl-*N*-maltopentaonocyl-L-glutamate (0.5 g, yield 59%) as a white powder. IR (KBr): 1736 cm^{-1} [ν(C=O)]; ^{1}H-NMR ([$^2H_6$]DMSO, 200 MHz): δ 0.8 (6H), 1.2 (60H), 1.5 (4H), 2.0 (2H), 2.3 (2H), 2.7– ≈ 6.0 (56H), 7.9 (1H).

Experimental

Materials

Maltotriose was purchased from Wako Pure Chemical Industries, maltopentaose and maltoheptaose were purchased from Nihon Shokuhin Kako Co. L-Glutamic acid was purchased from Kanto Chemical Co. 1-Bromotetradecane, 1-bromohexadecane, 1-bromooctadecane, and stearyl alcohol were purchased from Tokyo Kasei Kogyo Co. Concanavalin A was purchased from Seikagaku Co.

Glycolipids **1a**, **b**, and **c** were used to study the influence of the alkyl chain length on the assembling structures of the glycolipids. Glycolipids **1c**, **d**, and **e** were used to study the effect of oligosaccharide chain length on the assembling structures of the glycolipids. Glycolipids **1c** and **2** were compared to clarify the difference when amide and secondary amino linkages connect the hydrophilic and hydrophobic parts.

Study of monolayer films

A monolayer of the glycolipids was spread from a benzene/methanol (9/1 v/v) solution of the glycolipids on the subphase of pure water at 25 °C. A portion (50 μl) of the stock solution (2 mM) was applied with a microsyringe. The surface area was varied by moving a Teflon-coated barrier automatically at a rate of 14 cm^2 min^{-1} in a thermostated Langmuir trough (HBM-type balancemeter, Kyowa Interface Sci. Co.). The surface pressure (π) and area (A) were recorded with an X–Y recorder.

Measurement of critical micelle concentration (c.m.c.)

The c.m.c. was measured using an iodine solubilization method.[19] Various amounts of the synthetic glycolipids were dispersed into an iodine aqueous solution ([I_2] = 30 mg l^{-1}). The transmittance at the maximum absorption wavelength of 360 nm was measured by a UV–VIS spectrophotometer

(MPS-2000, Shimadzu Co.). The relationship between the glycolipid concentration and the logarithm of the transmittance was obtained to determine the c.m.c. from the inflection point of the relation.

Differential scanning calorimetry (DSC)

An aqueous dispersion of the sample ([glycolipid] = 6.8 mM, 60 μl) was sealed into a silver pan. DSC analysis was performed with a Seiko 120 DSC from 10 to 80 °C at a scan rate of 2 °C min^{-1}.

Transmission electron microscopy (TEM)

The synthetic glycolipids were dispersed into pure water above their phase transition temperatures (T_c). An aqueous solution of ammonium molybdate (5 wt.%, 600 μl) or phosphotungstic acid (2 wt.%, 600 μl) was mixed with the dispersion (600 μl) and incubated at 25 °C for 12 h. One drop of the mixed solution was dropped onto a carbon-coated copper grid (Jeol Datum Co.), and then the excess solution was immediately removed with the help of a filter paper. The grid was kept in a desiccator for 12 h and was then observed by TEM (JEM-100CX, Jeol Co.) using an acceleration voltage of 100 kV.

Cryo-transmission electron microscopy (cryo-TEM)

Thin vitrified films of the glycolipid dispersion, spanning the holes in a carbon foil, were generated, after blotting the excess solution, by shooting the grid from the controlled environmental vitrification system (CEVS) through a synchronized shutter mechanism into a liquid ethane container held at 89 K. A Gatan cryo-transfer system and specimen holder (Model 626) were used to transfer the specimens to a Philips CM12 electron microscope where micrographs were taken while maintaining a temperature of −176 °C. At a defocus value of about 1.2 μm, used for imaging, the absence of phase contrast transfer reversals allows a straightforward interpretation of the ≈2 nm resolution results.

Atomic force microscopy (AFM)

The synthetic glycolipids were dispersed into pure water above T_c. One drop of the dispersion was dropped onto a mica surface, and then the excess dispersion was immediately removed with help of a filter paper. The surface of the mica was imaged with a Digital Instruments Nanoscope II scanning force microscope and software in air at room temperature.

^{1}H-NMR

Dimethyl sulfoxide (DMSO) was added to the sample D_2O dispersion ([glycolipid] = 2 mM) as an external reference ([glycolipid]/[DMSO] = 50/1 by mol). ^{1}H-NMR spectra were recorded on a Jeol JNM-LA500 spectrometer equipped with a thermal controller (Jeol Co.). The sample dispersion was heated from 25 to 70 °C.

Isothermal titration calorimetry (ITC)

ITC was performed using an Omega titration calorimeter (MCS ITC, Microcal, Inc.).[20] 5 μl of a Con A solution ([Con A] = 0.812 mM) was injected at an interval of 4 min from the computer-controlled 250 μl microsyringe into the **1c** dispersion (cell volume = 1.35 ml) at 25 °C while stirring at 400 rpm. A controlled experiment was performed by making an identical injection of the Con A solution in the absence of **1c**. The experimental data were fitted to the theoretical titration curve using software supplied by Microcal to yield the values for K (association constant) and ΔH (the enthalpy change).

Results

Monolayer studies

The area per molecule was measured from the surface pressure–area (π–A) isotherm as shown in Fig. 1. The results are summarized in Table 1. The point where the slope of the π–A isotherm increases gradually from zero with decreasing molecular area is assigned to the transition from gas to liquid phase. The point where the slope of the π–A isotherm increases steeply is assigned to the transition point from fluid to solid phase. The molecular area can be estimated from the extrapolation of this curve to zero surface pressure.[21]

The surface areas of the transition from gas to liquid phase for **1a–e** were estimated to be 102, 112, 103, 93, and 200 Å^2, respectively. It is of interest that **2** has a smaller transition surface area (80 Å^2) than **1c** (103 Å^2).

A second transition was not observed for **1a** and **1e**. The surface pressure of the usual bimolecular membrane was reported as 20– ≈ 30 mN m^{-1}.[22,23] The molecular area of glycolipids **1a–d** at 30 mN m^{-1} of surface pressure were 56.0, 59.0, 51.5, and 47.5 Å^2, respectively. *N*-Glycosidic lipid **2** showed a molecular area of 52 Å^2 at 30 mN m^{-1}, which was almost the same value as that of **1c** with the same length of oligosaccharide and alkyl chains.

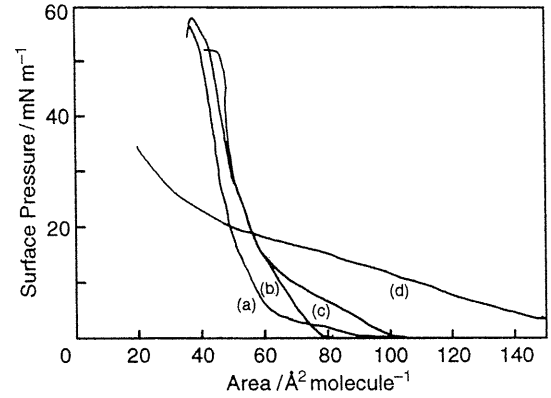

Fig. 1 Surface pressure–surface area (π–A) isotherms of: (a) **1d**, (b) **2**, (c) **1c**, and (d) **1e** at 25 °C

Table 1 Areas per molecule, collapse pressures of glycolipids, and physical properties of the glycolipid assemblies

glycolipid	molecular area at 30 mN m^{-1}[a]/Å^2	collapse pressure[a]/mN m^{-1}	c.m.c.[a]/mM	T_c/°C	ΔH/kJ mol^{-1}	assembling structure
1a	56.0	44.0	0.72	non	—	fiber
1b	59.0	51.1	0.47	45	20.1	large disk ($< T_c$), fiber ($> T_c$)
1c	51.5	52.3	0.0083	58	33.9	large disk, small disk, granule, and cone
1d	47.5	51.8	0.015	57	27.6	vesicle and large disk
1e	soluble	soluble	0.82	non	—	spherical micelle and short fiber
2	52.0	50.0	$<10^{-2}$	54	5.4	vesicle
				66	44.4	

[a] 25 °C in pure water.

Critical micelle concentrations (c.m.c.s)

The c.m.c.s of **1a–c** in pure water at 25 °C were 7.2×10^{-4}, 4.7×10^{-4}, and 8.3×10^{-6} M, respectively (Table 1). It is indicated that the c.m.c. decreases with increasing alkyl chain length. The c.m.c. of **1b** is very high in comparison with the c.m.c. (10^{-10} M) of dipalmitoylphosphatidylcholine (DPPC), which has the same alkyl chain length.[24] The c.m.c.s of **1d** and **e** were 1.5×10^{-5} and 8.2×10^{-4} M, respectively. From a comparison of the c.m.c.s among **1c–e**, which have the same alkyl chains (carbon number 18), the c.m.c. of **1e** with the longest saccharide chain showed the largest value of the three.

Gel-to-liquid crystalline phase transition temperatures (T_cs)

As shown in Table 1, no phase transition was found for the aqueous dispersions of **1a** and **1e** above their c.m.c.s, whereas, **1b–d** showed DSC peaks at 45, 58, and 57 °C with ΔH values of 20.1, 33.9, and 27.6 kJ mol^{-1}, respectively. As references, the T_c values of multilamellar vesicles, which consist of phospholipids with different alkyl chain lengths, such as dimyristoylphosphatidylcholine (DMPC), DPPC, and distearoylphosphatidylcholine (DSPC), are 24, 42, and 55 °C with ΔH values of 22.6, 36.4, and 44.4 kJ mol^{-1}, respectively.[25] The T_c values of the glycolipids were 2–3 °C higher compared with those of the phospholipids with the same alkyl chain length, whereas the ΔH values of the glycolipids were smaller than those of the corresponding phospholipids. A comparison of the T_c values of **1c** and **1d** showed no significant influence of the saccharide chain length on the phase transition temperature. *N*-Glycosidic lipid **2** has a pretransition at 54 °C of $\Delta H = 5.4$ kJ mol and a main transition at 66 °C of 44.4 kJ mol^{-1}.

Studies of assembling structure of the glycolipids

The amidic glycolipid powder **1a** (14,5) was dispersed in pure water at 25 or 60 °C and formed transparent solutions. It took a fiber-like structure, which was observed by cryo-TEM, as shown in Fig. 2(a). The fibers have a ribbon-like organization, namely the thickness and width of the ribbon were 8.4 nm and 10 nm, respectively.

The solid material of **1b** (16,5) could not be dispersed into a stable solution in water at 25 °C, below the T_c (45 °C), however, it formed a stable transparent solution when dispersed at 60 °C. It became turbid when the solution at 60 °C was cooled down to 25 °C. The transparent solution above the T_c was found to be a dispersion of fibers with a thickness of 10 nm, and the turbidity below the T_c was caused by the generation of large disks, mostly in the size range of 200 nm [Fig. 2(b)]. The structural changes were fully temperature reversible. Closer inspection of the stained or vitrified samples revealed the existence of brims at the edge of the disk. AFM was used to confirm this structure and the bilayer thickness.[26] The average thickness of the bilayer disks on the mica surface was found to be 5.3 nm. However, the brim was not confirmed in the AFM pictures [Fig. 2(c)]. The observed thickness of the disk was small compared with the bilayer membrane. This might be owing to the interaction of the disk with the hydrophilic surface of mica.

When glycolipid **1c** (18,5) was dispersed into water at 60 °C, a turbid dispersion was obtained. TEM micrographs using a negative staining method showed that large disks with an average diameter of 400 nm were mainly present, as shown in Fig. 3(a). The average thickness of 35 individual large disks on a carbon-coated flat collodion membrane was found to be 9 ± 1 nm by AFM. This value agreed well with the bilayer thickness of **1c** (10 nm), assuming an all-*trans* conformation based on a CPK model. It is of interest that the large disk shape changed to a fiber-like structure when a 0.1% aqueous urea solution was added to disrupt the hydrogen bonding.

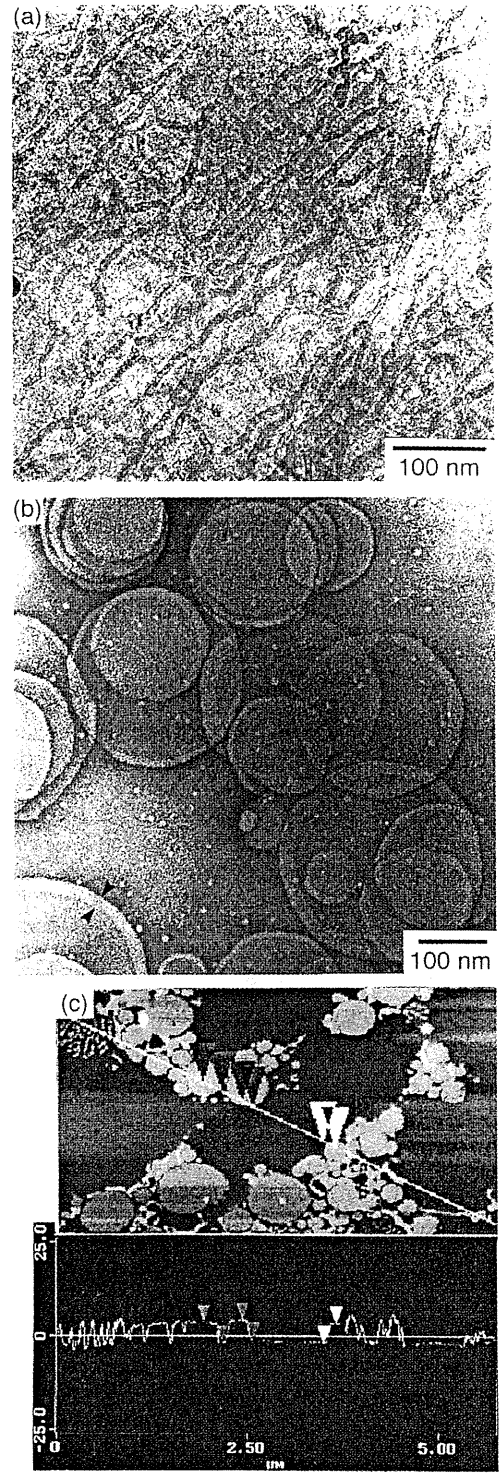

Fig. 2 Microscopic observation of glycolipid assemblies: (a) cryo-TEM of fiber-like assemblies (**1a**), (b) TEM of large disk-like assemblies (**1b**) below T_c, and (c) AFM of large disk-like assemblies (**1b**) below T_c

We obtained similar small disks with an average diameter of 50 nm by extrusion of the **1c** dispersion through the isopores of polycarbonate membrane filters (by changing the pore size in a stepwise manner from 3.0 μm to 50 nm). After ultracentrifugation at 100 000*g* for 30 min, we obtained small disk-, rod-, and cone-like assemblies in the supernatant with a total yield of 45 wt.% The average diameter and the thickness of the small disk, from AFM, were 40 nm and 8 nm, respectively. Fig. 3(b) are the same areas of a negatively stained TEM sample but with a change in the observation angle of 45°. Though the axial length and diameter of the rod are around

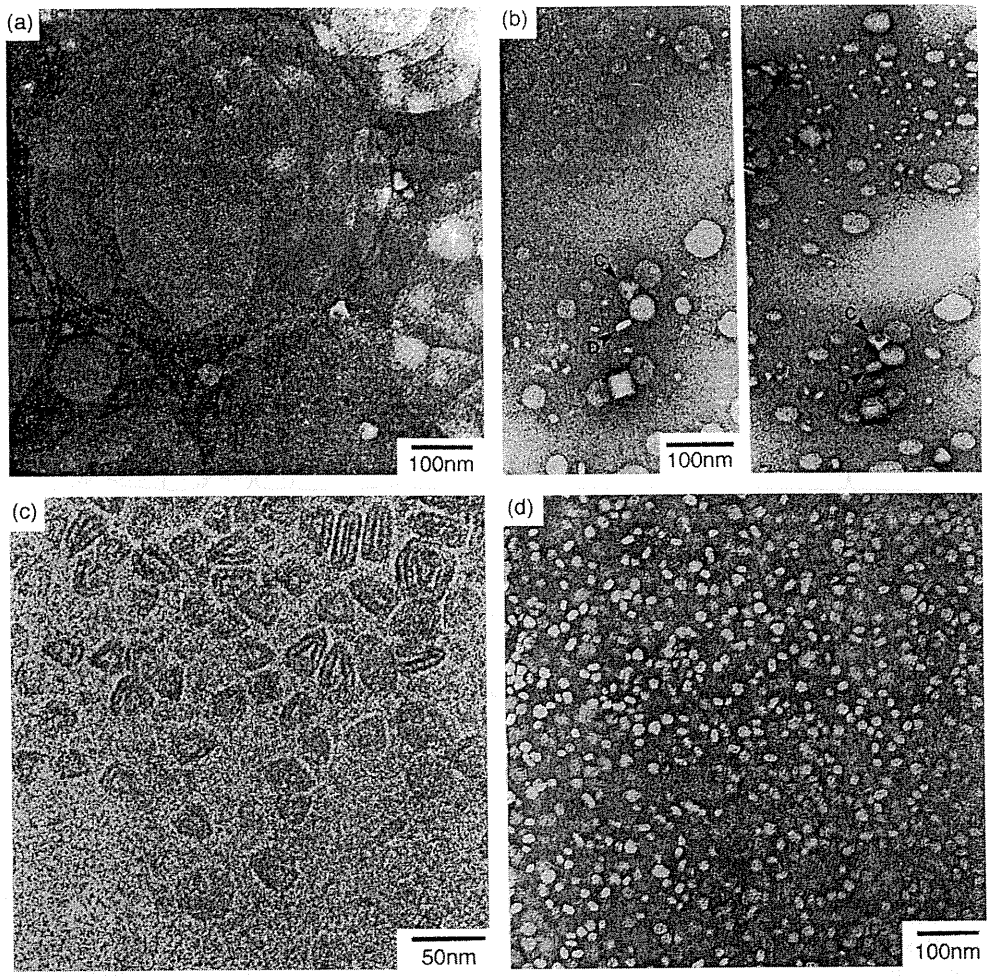

Fig. 3 Microscopic observation of glycolipid assemblies (**1c**): (a) TEM of large disk-like assemblies; (b) two TEMs of small disk-like assemblies changing the observation angle by 45°, arrows C and D in the pictures indicate cone- and disk-like assemblies, respectively; (c) cryo-TEM of small disk- and cone-like assemblies; (d) TEM of granule-like assemblies

40 nm and 11 nm, respectively, a careful analysis of the rod-like assemblies, using high contrast, suggests that some of the rods are identified with the edge part of the disks. The axial length of the rod corresponds to the diameter of the disk, and the rod becomes an ellipsoid-like structure by changing the observation angle. The TEM pictures also disclosed the existence of cone-like structures, and some of the disks turn out to be the bottom of the cone. The close-up image of vitrified **1c** shown in Fig. 3(c), provided a detailed image of the cone in an aqueous dispersion. The thickness of the shell of the cone is *ca.* 8 nm, which corresponds to the thickness of the bilayer. Large cracks were observed in the cryo-image at the edge parts of the cone.

Sonication (a probe type sonicator, 80 W, 15 min, 4 °C) of the dispersion of glycolipid **1c** yields a transparent solution. It was a mixture of a granule-like structure and disks (100–$\approx$ 200 nm diameter). The granule-like structure was separated off in the supernatant by ultracentrifugation at 100 000*g* for 30 min with 25 wt.% yield. In this case, neither disk-, rod-, nor cone-like structures were confirmed. The average long and short diameters of the grain were 18 and 9 nm, respectively [Fig. 3(d)].

As summarized in Table 1, glycolipid **1d** (18,3) could be dispersed only above 60 °C to form a mixture of vesicles (average diameter 250 nm and yield 32%) and disk-like structures (average diameter 104 nm and yield 68%). The dispersion was not stable and easily precipitated. On the other hand, glycolipid **1e** (18,7) was easily dispersed at any temperature, and formed small disks (average diameter 54 nm) and spheres (average diameter 8 nm) or short fiber-like (average diameter 8 nm and length 40 nm) structures.

It is noted that *N*-glycosidic lipid **2** (18,5) took a normal unilamellar vesicular structure of 174 ± 71 nm diameter, which is quite different from the large disk-like structure of **1c** (18,5) under the same preparation condition.

Temperature dependence of ^{1}H-NMR of glycolipid assemblies

In ^{1}H-NMR spectroscopy, the increase in the peak intensity or the narrowing of the half-width reflects the increase in the segmental motion of the objective molecule.[27] We studied three samples of the same glycolipid **1c**, (i) the hydrate at 60 °C mainly containing large disks, (ii) the ultracentrifuged supernatant of an extruded fluid containing small disks, cones *etc.*, and (iii) the ultracentrifuged supernatant of a sonicated sample containing granule-like particles. Those samples correspond to the samples in Fig. 3(a), (b), and (d), respectively.

For preparation (i), which contains large disks, neither the saccharide chain nor the alkyl chain were confirmed below the T_c [Fig. 4(a)]. Only a small peak of alkyl chains (δ 0.8, 1.2) appears above the T_c, which increases with temperature. However, the peaks for the saccharide chain (δ 3.2–$\approx$ 4.0) were hardly detected. A quite different profile was observed for preparation (ii), namely both the saccharide and alkyl chains appear as broad peaks even below the T_c [Fig. 4(b)]. The saccharide chain peaks gave significantly higher resolution compared with those of alkyl chains at low temperatures. The peak intensity of the alkyl chains increased with temperature, and well-resolved peaks were obtained above the T_c. The granule-like micellous structure [preparation (iii)] gives well-resolved peaks for both the saccharide and alkyl chains even well below the T_c [Fig. 4(c)].

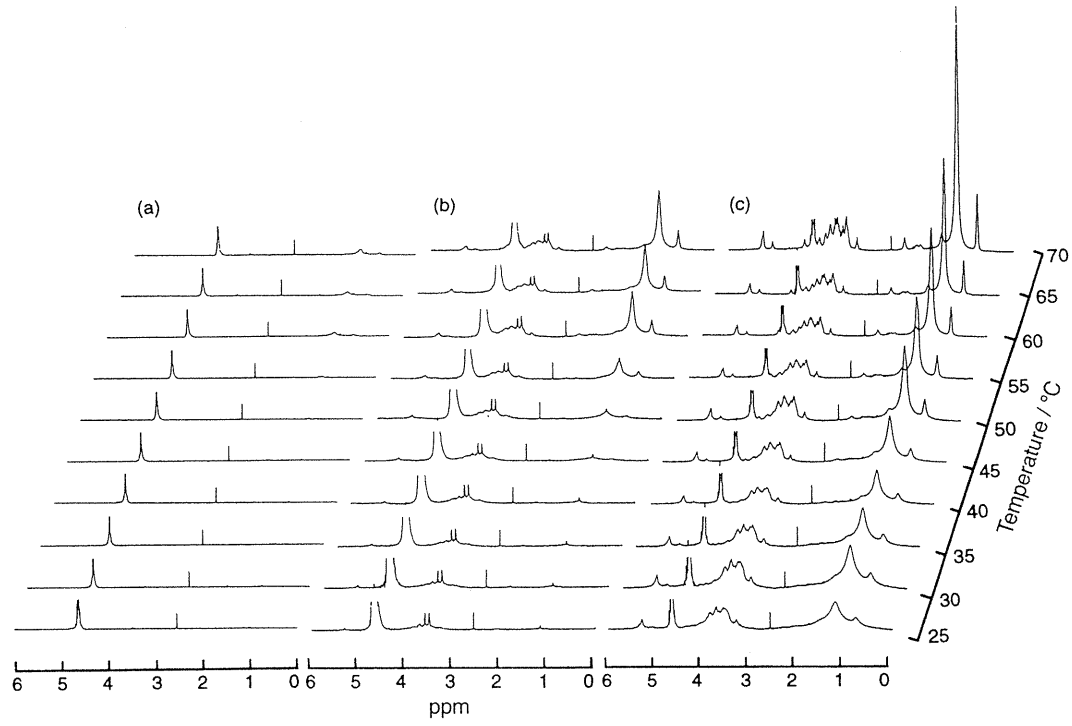

Fig. 4 Segmental motion of glycolipid assemblies observed from the temperature dependence of ^{1}H-NMR spectra of D_2O dispersions: (a) preparation (i), containing mainly large disk-like assemblies as shown in Fig. 3(a); (b) preparation (ii), containing mainly small disk-like assemblies as shown in Fig. 3(b); and (c) preparation (iii), containing mainly granule-like assemblies as shown in Fig. 3(d)

The intensity and sharpness of the peaks attributed to the alkyl chains increases steeply compared with those of the saccharide chains. It should be noted that no phase transition behavior was observed.

Thermodynamic analysis of glycolipid assemblies complexed with Con A

To study the function of glycolipid assemblies, a solution of Con A (which recognizes the terminal part of the saccharide chain) was added dropwise to the glycolipid preparations (i), (ii), and (iii). The enthalpy change was monitored by microcalorimetry. Preparation (i) showed a very small exothermic peak per injection in comparison with (ii) and (iii). The difference was reflected in the apparent binding ratio of glycolipid **1c** to Con A. The binding ratio of the large disks was more than ten times that of the granule-like structure, as summarized in Table 2. The binding constant and enthalpy change for preparations (i) and (iii) were almost the same and both were larger than (ii). These results suggest that preparation (ii) binds with Con A in a different way to preparations (i) and (iii).

Stability of glycolipid assemblies as a dispersion state

Aggregation and fusion were not observed for small disks or granules. No spontaneous change was observed in turbidity and morphology within three months or longer periods at room temperature. The large disks were converted to small ones when the temperature was above the T_c.

A lyophilized powder of the small disks could be redispersed into pure water above the T_c. The preservation of the original disk-like structure after redispersion was confirmed by TEM observation. The granule-like structure, on the other hand, was not preserved after the freeze-drying and rehydration process. The granules fused to change into small disks.

Discussion

A series of glycolipids (*m*,*n*) having two alkyl chains was synthesized, and their assembling structures were studied in relation to the number of carbons (*m*) in the alkyl chains and the saccharide unit (*n*) of the oligosaccharide chain. For **1a** (14,5) and **1e** (18,7) the portion of the oligosaccharide chain of the glycolipid is too high to give stable molecular packing in a self-assembled state, resulting in the lack of a phase transition temperature. The low collapse pressure of the **1a** monolayer (Table 1) compared with the other glycolipids could be explained from the lack of cohesion at high pressure, *i.e.*, **1a** could not form a solid monolayer membrane at an air/water interface or in an aqueous system.

Glycolipid **1b** (16,5) took a fiber-like structure above the T_c and a disk-like structure below the T_c, whereas **1c** (18,5), prepared by hydrating the powder above the T_c, formed a large disk-like structure independently of temperature. The relatively low molecular packing of the **1b** assemblies above the T_c should result in the conversion of disks to fibers. The c.m.c. of glycolipid **1c** with the same alkyl chain length is very high (8.3×10^{-6} M) relative to a phospholipid with two alkyl chains, such as DSPC, which is less than 10^{-10} M. Such a high c.m.c. should enable **1c** to take various structures by changing

Table 2 Thermodynamic parameters of the binding of Con A to various glycolipid assemblies at 25 °C

preparation	main assembling structure	binding ratio (glycolipid/Con A)	binding constant, K/M^{-1}	ΔH/kJ mol^{-1}
(i)	large disk	*ca.* 303	$(6.1 \pm 1.6) \times 10^4$	-93.7 ± 169.9
(ii)	small disk	43.5 ± 0.9	$(2.6 \pm 0.4) \times 10^4$	-67.8 ± 15.9
(iii)	granule	25.9 ± 2.0	$(5.8 \pm 0.9) \times 10^4$	-108.4 ± 10.5

the preparation conditions, such as temperature and shear stress, because dissociation and reorganization would occur easily.

Glycolipid **1c** took a thermodynamically stable large disk-like structure with bimolecular thickness, while glycolipid **1d** (18,3) took an unstable mixture of large disks and vesicles. Israelachvili *et al.*[28] have defined a packing parameter P ($= v/a_0 l_c$) which related to the geometric shape of the amphiphile molecule, where v is the volume of the hydrocarbon chain, a_0 is the optimal surface area per head-group, and l_c is the length of the alkyl chain. The relationship between P and the assembling structure was theoretically defined ($P < 1/3$ = spherical micelle; $1/3 < P < 1/2$ = cylindrical micelles; $1/2 < P < 1$ = bilayer, vesicle; ≈ 1 = planar bilayer, $P > 1$ = inverted micelle). The P values of **1c** at 20 and 30 mN m^{-1} were 0.93 and 1.02, and those of **1d** were 1.03 and 1.11, respectively. This showed that **1c** can form a stable bilayer but **1d** cannot.

Interestingly, **2** which has an amino group instead of the amide group, forms a vesicular structure. The only difference between **1** and **2** is the way of coupling the saccharide chain to the dialkyl groups. The hydrogen bond of the amide groups of **1** should mainly characterize the assembling structure. **1c** and **2** have almost the same molecular area at the same surface pressure, but **1c**, which has an amide bond, would be able to take a higher surface pressure and tighter packing due to its hydrogen bonding. The importance of the hydrogen bonding of the amide group in making the large disk-like structure was supported by the result that a fiber-like structure was confirmed when glycolipid **1c** was dispersed into an aqueous urea solution.[29] This results from the disruption of the hydrogen bonding among the glycolipids at the amide linkage, meaning that the hydrogen bonding at the amide groups of **1c** are necessary in forming the large disk-like structure.[30]

The assembling structure of the glycolipids significantly depends on the preparation methods and condition. For example, the large disks of glycolipid **1c** prepared by hydration at 60 °C, changes to the smaller disk-, cone-, or granule-like structures, depending on the degree of energy applied during preparation, such as mechanical mixing, shear stress, or sonication. High energy irradiation makes very small granule-like assemblies with a high proportion of edge,[31] and it is interesting that such assemblies are stable for the long term. For phospholipid vesicles, small vesicles prepared by sonication are generally unstable and tend to aggregate and fuse into larger and more stable vesicles.[32] Therefore, the high stability of the small assemblies with very high curvature should lead to a high stability of the edge part of the disk- or rod-like assemblies.

The assembling structures of the glycolipids were characterized in terms of 'bimolecular thickness,' 'closed molecular packing at the planar membrane,' and 'loose molecular packing at the edge.' For example, the large disk-like structure is thought to be a planar membrane with a small portion of edge part, and the small disk a planar membrane with a high portion of edge. The fiber-, rod-, and granule-like structures consist entirely of molecular packing at the edge portion. The cone-like structure has a shell with bilayer thickness and resembles a vesicular structure having a single bilayer membrane, but it has both planar and edge parts. However, the detailed structure and mechanism of its generation has not been clarified yet.

In general, the disk-like assemblies form in mixed systems,[33–39] in this case, the components of the planar and edge portions are different, *i.e.*, the planar portion is formed by the components that can form the bilayer structure, and the edge portion is stabilized by components with large hydrophilic head-groups or short alkyl chains, which cannot form stable bilayer packing;[40] the edge portion is thermodynamically unstable.[41,42] However, for our glycolipids, the disks were formed by single components. It can be proposed that the planar and edge portions are stabilized by the different packing conditions of the single glycolipid, *i.e.*, the packing at the edge has extremely high curvature and is stabilized by the existence of the large non-ionic and hydrated head-groups of the glycolipid, and the high stability of the plane is due to the high packing of the saccharide chains from hydrogen bonding and the steric hinderance of the large head-group, which do not allow a convex surface.

The molecular packing of preparation (ii), containing small disks, is quite different from that of preparation (i), with large disks. By DSC measurement, the small disk has a T_c of 48.5 °C, lower than that of the large disk (58 °C), and its enthalpy difference (4.2 kJ mol^{-1}) is smaller and broader than that of the large one (33.9 kJ mol^{-1}). This suggests the large distribution of the glycolipid packing. Similar results were also obtained from the ^{1}H-NMR study. It should be noted that the molecular packing around the edge of the disk is disturbed even in the gel phase because the high curvature of the edge has high mobility so that the saccharide chains cover all of the surface, even around the edge. Such disturbed and loose packing should become tighter and more oriented toward the center of the disk.[40] Therefore, the molecular packing of the assemblies decreases with an increasing ratio of edge to the entire assembly. This differentiates the small disk from the large disk. The large amount of edge of the small disk and its relatively loose packing of the saccharide chain resulted in the high reactivity of the chain with Con A. The smaller ΔH and K in Table 2 suggest that the saccharide chains in the plane with the smaller reactivity should participate in complexation.

On the other hand, the granule-like structure showed a broad phase transition at 48 °C, and a small endothermic peak of 6.3 kJ mol^{-1}. It is easily concluded that all glycolipid molecules should be packed like the edge portion of the disk. In ^{1}H-NMR spectroscopy, the mobility of the glycolipid in the granule-like assembly is the highest of the three and increases steeply from a temperature lower than the value of T_c observed for the large disk. Therefore, the low molecular packing resulted in the high reactivity with Con A. A high concentration of the chains seems to be necessary to bind because Con A has four binding sites for saccharide chains.[43] However, the tight packing of the chains would reduce the reactivity owing to the steric hindrance of the chains.[44]

Conclusion

Glycolipid **1** mainly takes two stable molecular assemblies; one is a planar bimolecular membrane stabilized by hydrogen bonding at the amide linkage and by hydrophobic interaction of alkyl chain; the other is a micelle structure, such as micelle fibers and granules, stabilized by the high segmental motion of the oligosaccharide chain and alkyl chains. The polymorphism of the glycolipid should be determined from the balance of the two packing states.

The reactivity of the saccharide chains against saccharide-recognizing proteins, such as Con A, is influenced by the saccharide chain packing. Loose packing at the edge is important for complexation of the saccharide chains with Con A. Similar properties can occur on biological cell surfaces containing glycolipid or glycoprotein, where free space between the saccharide chains is not obtained by curvature but by branching of the saccharide chains.

This work was partially supported by a project of the Material Research Laboratory for Bioscience and Photonics in Waseda University and a Grant-in-Aid from ARISE, WU (Glycolipid #246), the Cosmetology Research Foundation and by SHB-312 Vectorial Membrane Process. The work at the Freie Universität Berlin was partially carried out as a German–Japanese Cooperative Research Project of DHG-JSPS.

References

1 *New Comprehensive Biochemistry, Vol. 10, Glycolipids*, ed. H. Wiegandt, Elsevier, Amsterdam, New York, Oxford, 1985.
2 W. Curatolo, *Biochim. Biophys. Acta*, 1987, **906**, 137.
3 R. A. Dwek, *Chem. Rev.*, 1996, **96**, 683.
4 B. Maggio, T. Ariga, J. M. Sturtevant and R. K. Yu, *Biochemistry*, 1985, **24**, 1084.
5 G. D. Fidelio, B. Maggio and F. A. Cumar, *Biochim. Biophys. Acta*, 1986, **854**, 231.
6 B. Maggio, J. Aldert and R. K. Yu, *Biochim. Biophys. Acta*, 1988, **945**, 145.
7 M. Hato and H. Minamikawa, *Langmuir*, 1996, **12**, 1658.
8 K. Tamada, H. Minamikawa, M. Hato and K. Miyano, *Langmuir*, 1996, **12**, 1666.
9 K. Endo, K. Inoue and S. Nojima, *J. Biochem.*, 1982, **92**, 953.
10 W. Curatolo, *Biochim. Biophys. Acta*, 1987, **906**, 111.
11 D. A. Mannock, R. N. A. H. Lewis, A. Sen and R. N. McElhaney, *Biochemistry*, 1988, **27**, 6852.
12 H. J. Hinz, H. Kuttenreich, R. Meyer, M. Renner and R. Fründ, *Biochemistry*, 1991, **30**, 5125.
13 C. Guedj, B. Pucci, L. Zarif, C. Coulomd, J. G. Riess and A. A. Pavia, *Chem. Phys. Lipids*, 1994, **72**, 153.
14 R. Koynova and M. Caffrey, *Chem. Phys. Lipids*, 1994, **69**, 181.
15 S. Takeoka, H. Sakai, H. Ohno, K. Yoshimura and E. Tsuchida, *J. Colloid Interface Sci.*, 1992, **152**, 351.
16 S. Takeoka, H. Sakai, M. Takisada and E. Tsuchida, *Chem. Lett.*, 1992, **1992**, 1877.
17 H. Sakai, M. Takisada, S. Takeoka and E. Tsuchida, *Chem. Lett.*, 1993, **1993**, 1891.
18 P. Denkinger, W. Burchard and M. Kunz, *J. Phys. Chem.*, 1989, **93**, 1428.
19 S. Ross and J. P. Oliver, *J. Phys. Chem.*, 1959, **63**, 1671.
20 T. Wiseman, S. Williston, J. F. Brandts and L-N. Lin, *Anal. Biochem.*, 1989, **179**, 131.
21 *Membrane Mimetic Chemistry*, ed. J. H. Fendler, Wiley, New York, 1982, p. 78.
22 A. Blume, *Biochem. Biophys. Acta*, 1979, **557**, 32.
23 A. J. C. Fulford and W. E. Pell, *Biochim. Biophys. Acta*, 1980, **598**, 237.
24 R. Smith and C. Tanford, *J. Mol. Biol.*, 1972, **67**, 75.
25 *Membrane Mimetic Chemistry*, ed. J. H. Fendler, Wiley, New York, 1982, p. 136.
26 G. Binnig and C. F. Quate, *Phys. Rev. Lett.*, 1986, **56**, 930.
27 H. C. Jarrell, A. J. Wand, J. B. Giziewicz and I. C. P. Smith, *Biochim. Biophys. Acta*, 1987, **897**, 69.
28 J. N. Israelachvili, D. J. Mitchell and B. W. Ninham, *J. Chem. Soc., Faraday Trans. 2*, 1976, **72**, 1525.
29 A. Polidori, B. Pucci, L. Zarif, J-M. Lacombe, J. G. Riess and A. A. Pavia, *Chem. Phys. Lipids*, 1995, **77** , 225.
30 *Membranes and Molecular Assemblies: The Synkinetic Approach*, ed. J. H. Fuhrhop and J. Köning, The Royal Society of Chemistry, Cambridge, 1994, p. 98.
31 C. Cecutti, B. Focher, B. Perly and T. Zemb, *Langmuir*, 1991, **7**, 2580.
32 M. Wong, F. H. Anthony, T. W. Tillack and T. E. Thompson, *Biochemistry*, 1982, **21**, 4126.
33 T-L. Lin, C-C. Liu, M. F. Roderts and S-H. Chen, *J. Phys. Chem.*, 1991, **95**, 6020.
34 J. Bian and M. F. Roberts, *Biochemistry*, 1990, **29**, 7928.
35 M. Ollivon, O. Eidelman, R. Blumenthal and A. Walter, *Biochemistry*, 1988, **27**, 1695.
36 S. Almog, T. Kushnir, S. Nir and D. Lichtenberg, *Biochemistry*, 1986, **25**, 2597.
37 P. Schurtenberger, N. Mazer and W. Kanzig, *J. Phys. Chem.*, 1985, **89**, 1042.
38 P. Fromherz and D. Ruppel, *FEBS Lett.*, 1985, **19**, 155.
39 J. Dufourcq, J-F. Faucon, G. Fourche, J-L. Dasseux, M. L. Maire and T. Gulik-Krzywicki, *Biochim. Biophys. Acta*, 1986, **859**, 33.
40 T-L. Lin, *J. Colloid Interface Sci.*, 1992, **154**, 444.
41 P. Fromherz, C. Rocker and D. Ruppel, *Faraday Discuss. Chem. Soc.*, 1986, **81**, 39.
42 S. Ljunggren and J. C. Eriksson, *J. Chem. Soc., Faraday Trans. 2*, 1986, **82**, 913.
43 J. W. Becker, G. N. Reeke, Jr., B. A. Cunningham and G. M. Edelman, *Nature (London)*, 1976, **259**, 406.
44 Y. Ebara and Y. Okahata, *J. Am. Chem. Soc.*, 1994, **25**, 11209.

Paper 8/00289D; *Received 9th January*, 1998

ART. CELLS, BLOOD SUBS., AND IMMOB. BIOTECH., 26(5&6), 497-506 (1998)

EFFECTS OF THE pH-CONTROLLED HEMOGLOBIN VESICLES BY CO_2 GAS

SungIck Park, Takehiro Kose, Masaomi Hamasaki, Shinji Takeoka,
Hiroyuki Nishide and Eishun Tsuchida*
Department of Polymer Chemistry, ARISE
Waseda University, Tokyo 169-8555, Japan.

Abstract: The hemoglobin vesicle (HbV) is a red cell substitute encapsulating purified concentrated Hb in a phospholipid vesicle. In order to improve the oxygen carrying capability of HbV, the pH value of the Hb solution should be adjusted to 7.0 in the HbV preparation, and then the pH value should be adjusted to 7.4 where HbV functions as an oxygen carrier, because the maximum value of [Hb]/[Lipid] was obtained in which the pH of the Hb solution was 7.0, and the metHb formation rate was suppressed in the pH 7.4. Generally, the pH control of the inner aqueous phase of HbV is difficult by changing the pH in the outer phase. We could control the pH of the Hb solution from 7.4 to 7.0 by dissolving CO_2 into the Hb solution, and after the preparation of HbV, the pH of HbV is changed to 7.4 by reducing the pressure. The resulting pH-controlled HbV by CO_2 gas showed a high [Hb]/[Lipid] value of 1.7 with a low rate of metHb formation.

INTRODUCTION

The hemoglobin vesicle (HbV), which has a cellular structure encapsulating a purified concentrated Hb solution, is expected to be one candidate for artificial red cells [1-3]. In order to improve the oxygen carrying capability of HbV, one must 1) increase the concentration ratio of Hb to total lipid components of the vesicles ([Hb]/ [Lipid]), 2) chemically stabilize an encapsulated Hb solution, namely the suppression of metHb formation (Hb in a ferrous state is changed to the ferric state and loses its oxygen binding ability), and 3) regulate the oxygen affinity of HbV to 27 Torr which resembles the red cell.

*To whom all the correspondence should be addressed.

Concerning 1), during the extrusion procedure for the preparation of HbV, the pH value of the Hb solution should be regulated to 7.0 which is near the isoelectric point of Hb (p*I* = 7.02, 25°C) [4]. With regard to 2), metHb formation would be more suppressed in the higher pH region than in the lower pH region, and it is more desirable for the pH value to be adjusted to a physiological value (7.4). Finally, concerning 3), the appropriate pH value is 7.4 because oxygen affinity decreases with lower pH values. Therefore, the pH value of the Hb solution should be adjusted to 7.0 in the preparation of HbV and 7.4 in which HbV functions as an oxygen carrier.

Generally, the pH control of the inner aqueous phase of HbV is difficult by changing the pH in the outer phase. Permeabilities of H^+ and OH^- in the bilayer membrane are relatively high (permeabilities of H^+ and OH^- are 1.4×10^{-4} cm/s) [5], but the counter anion of H^+ and counter cation of OH^- are very slow, because ion permeability through the bilayer membrane is too low (i.e, permeabilities of Na^+ and Cl^- are about 10^{-13} and 10^{-11} cm/s, respectively) [6].

On the other hand, under constant temperature, carbon dioxide is dissolved in water in proportion to the partial pressure of carbon dioxide in accordance with Henry's law, resulting in the pH decrease. Therefore, during the preparation of HbV, the pH of the Hb solution was changed from 7.4 to 7.0 by dissolving carbon dioxide in the Hb solution, and after preparation of HbV, the pH of HbV is adjusted to 7.4 by removing the dissolved carbon dioxide by reducing the pressure.

In this paper, we confirmed that the pH of the Hb solution could be controlled by the partial pressure of carbon dioxide, and that the resulting HbV has a high performance such as a high [Hb]/[Lipid] value and a low rate of metHb formation.

MATERIALS AND METHODS

pH measurement of the inner aqueous phase of vesicle

8-Hydroxy-1,3,6-pyrenetrisulfonate (pyranine) was used as a pH-indicator, and the pH was calculated from the calibration curve: the ratio of fluorescent intensity at 455 nm to 405 nm (pyranine, λ_{em} = 510 nm) [7,8]. Pyranine was dissolved in a phosphate buffer solution (PBS) at 0.5 mM, and the lipid bilayer was composed of Presome PPG-I [a mixture of 1,2-dipalmitoyl-*sn*-glycero-3-phosphatidylcholine (DPPC), cholesterol, 1,2-dipalmitoyl-*sn*-glycero-3-phosphatidylglycerol (DPPG) (Nippon Fine Chem Co.) at a molar composition of 5/5/1]. The pyranine solution and the lipids were then mixed ([Lipid]=1.5 g/dL). After sizing with an extrusion method (final pore size of the membrane filter was 0.22 μm) and the removal of unencapsulated pyranine using ultracentrifugation, the resulting pyranine encapsulating vesicle was diluted with PBS at a pyranine concentration of 1 μM. During the process of dissolving carbon dioxide into the pyranine encapsulating vesicle, the change in the pH of the inner aqueous phase

was calculated from the calibration curve, and compared with the pH of the outer aqueous phase which was measured using a pH meter.

Measurement of the metHb in HbV

The HbV suspensions were incubated at 37°C and at the oxygen partial pressure of 149 Torr. About 5 μL of the sample was periodically pipetted out and added to a UV cuvette containing 3 mL of PBS. The deoxygenation of the sample using bubbling N_2 resulted in the presence of only deoxyHb and metHb. The percentage of metHb was calculated from the ratio of absorbance at 405 nm (metHb) and 430 nm (deoxyHb) in the Soret band. The HbV sample of 0% metHb (100% deoxyHb) was prepared by incubation of the sample with sodium dithionite under a N_2 atmosphere at 25°C for 2 h. The sample of 100% metHb was prepared via the metHb formation of HbNO. Nitric oxide gas was bubbled in the deoxygenated HbV suspension to form 100% HbNO (λ_{max} in the Soret band: 415 nm). Nitrogen gas was then bubbled through the suspension to expel the excess NO. Next, O_2 gas was bubbled through the sample to convert the HbNO to metHb (λ_{max}: 405 nm) [9].

Preparation of HbV by using CO_2 gas

The encapsulated carbonylhemoglobin (HbCO, *ca.* 38 g/dL) contained pyridoxal 5'-phosphate (PLP, 18 mM, Merck Co.) as an allosteric effector and DL-homocysteine (5 mM, Aldrich Chemical Co.) as a metHb reductant. The pH value of the Hb solution was regulated with sodium carbonate to 7.4 at 37°C. By dissolving the CO_2/N_2 mixed gas (Pco_2 = 130 Torr) into the Hb solution, and the pH was adjusted to 7.0 at 37°C. Presome PPG-I powder was dissolved in $CHCl_3$. α-tocopherol (Merck Co.) was then added to the mixture for a final molar composition of 5/5/1/0.1. A lipid film was prepared on the inner wall of a flask using a rotary evaporator and dried *in vacuo* for 48 h. After dispersing the lipid mixture into an Hb solution under CO_2/N_2 mixed gas (Pco_2 = 130 Torr) for 24 h at 4°C, the resulting multilamellar vesicles were sized using extrusion through membrane filters (final pore size of the membrane filters was 0.22 μm), and the suspension was extruded while keeping the pH of the solution at 7.0. After the extrusion procedure, the solution pH was adjusted to 7.4 by removing carbon dioxide by reducing the pressure. After the removal of unencapsulated Hb using ultracentrifugation (50,000*g*, 40 min), the resulting HbV was diluted with saline to an Hb concentration of 0.5 g/dL. HbCO was converted to HbO_2 by visible light irradiation under an O_2 atmosphere [10]. After ultracentrifugation, the HbV was redispersed into PBS.